UNIVERSITAT POLITÈCNICA DE VALÈNCIA

ESCUELA TÉCNICA SUPERIOR INGENIEROS INDUSTRIALES VALENCIA

FINAL MASTER'S DEGREE THESIS IN BIOMEDICAL ENGINEERING

ANALYSIS OF THE BIOMECHANICAL BEHAVIOUR OF HEALTHY, DEGENERATED AND PMMA CEMENTED PIG LUMBAR INTERVERTEBRAL DISCS USING FINITE ELEMENT METHODS

AUTHOR: GUILLERMO COLLADO SORIA

SUPERVISOR: MARÍA JOSÉ RUPÉREZ MORENO

Academic Year: 2019-20

Acknowledgments

Me gustaría dar las gracias a todos mis familiares que han estado apoyándome durante todo mi recorrido académico, en especial a mi madre y a mi hermano, y a mi padre, el cual estaría muy orgulloso de mis proezas.

A todos mis amigos de la infancia y compañeros de Universidad, especialmente a Toni, quien durante estos últimos 5 años me ha ayudado y compartido buenos momentos conmigo.

Gracias a María José por ser la tutora de mi proyecto y por guiarme y ayudarme en todo momento.

Finalmente, me gustaría hacer mención especial a mis abuelos, los cuales han estado durante esta pandemia por Covid-19 aislados y alejados de la familia, les mando muchos ánimos y espero poder verlos pronto.

Abstract

As a continuation of the Final Degree Project carried out last year, the object of study deals with the comparison of porcine vertebrae in healthy, degenerated and cemented by polymethyl methacrylate (PMMA) conditions through Finite Element Method (FEM) simulation.

The objective is to compare the results of vertebrae strain and range of motion in different conditions: flexion, extension and lateral flexion, to study the possible causes of the Lower Back Pain (LBP) and the influence of an incision in the annulus fibrosus through the FEM simulations as it was developed previously through the Digital Image Correlation (DIC). The main purpose of this approach is to solve some of the main limitations of the experimental tests carrying out in the previously developed Final Degree Project, such as cost reduction or the use of animals' samples, and thus carrying out a research free of ethical dilemmas and the complexity of biomechanical facilities.

Keywords: Lower Back Pain, biomechanics, spine, lumbar vertebrae, intervertebral disc, degeneration, Finite Element Method.

Resumen

Como continuación del Trabajo de Fin de Grado realizado el año pasado, el objeto de estudio trata de la comparación de vértebras porcinas en condiciones sanas, degeneradas y cementadas mediante polimetil metacrilato (PMMA) mediante simulación por el Método de los Elementos Finitos (MEF).

El objetivo es comparar los resultados de deformación vertebral y rango de movimiento en diferentes condiciones: flexión, extensión y flexión lateral, para estudiar las posibles causas del dolor lumbar (LBP) y la influencia de la incisión en el anillo fibroso a través de las simulaciones FEM como se desarrolló previamente a través del Digital Correlación de Imágenes (DIC). El objetivo principal de este enfoque es solucionar algunas de las principales limitaciones de las pruebas experimentales que se llevan a cabo en el Trabajo Fin de Grado desarrollado anteriormente, como la reducción de costes o el uso de muestras de animales, y así realizar una investigación libre de dilemas éticos y la complejidad de las instalaciones biomecánicas.

Palabras clave: dolor lumbar, biomecánica, columna vertebral, vértebras lumbares, disco intervertebral, degeneración, Método de los Elementos Finitos.

Resum

Com a continuació del Treball de Fi de Grau realitzat l'any passat, l'objecte d'estudi tracta de la comparació de vèrtebres porcines en condicions sanes, degenerades i cimentades aplicant polimetil metacrilat (PMMA) mitjançant la simulació pel Mètode dels Elements Finits (MEF).

L'objectiu és comparar els resultats de deformació vertebral i rang de moviment en diferents condicions: flexió, extensió i flexió lateral, per estudiar les possibles causes de dolor lumbar (LBP) i la influència de la incisió en l'anell fibrós a través de les simulacions FEM com es va desenvolupar prèviament a través del Digital Correlació d'Imatges (DIC). L'objectiu principal d'aquest enfocament és solucionar algunes de les principals limitacions de les proves experimentals que es duen a terme en el Treball Fi de Grau desenvolupat anteriorment, com la reducció de costos o l'ús de mostres d'animals, i així realitzar una investigació lliure de dilemes ètics i la complexitat de les instal·lacions biomecàniques.

Paraules clau: dolor lumbar, biomecànica, columna vertebral, vèrtebres lumbars, disc intervertebral, degeneració, Mètode dels Elements Finits.

INDEX

FINAL MASTER'S DEGREE THESIS CONTENTS

I. Thesis
II. Budget
III. Appendix

DOCUMENT I: THESIS

DOCUMENT II: BUDGET

DOCUMENT III: APPENDIX

THESIS

1. INTRODUCTION

1.1. Spine properties, components and issues

In terms of human anatomy, the spine is a structural part of the body made of an ensemble of bones whose function is to provide support of the upper body weight, to protect the vital organs and the spinal cord and to provide mobility and stability [1]. For the rest of animals, the number of vertebrae and shapes can change, being one of the most remarkable differences the standing up of the human being.

Over time, those functions entail a long-term spine deterioration which debilitates the spine and the properties of its components, and this could lead for what is commonly known as the Lower Back Pain (LBP), especially in the elderly. For years, some studies have demonstrated that this issue is reported frequently with the age of the person [2] [3].

Regarding the LBP, it has been documented a correlation with the intervertebral disc degeneration [4], the aging [3] [5], body posture [6], fatigue due to repetitive loads common in physical effort jobs [3] [5] and also genetical influences that entail to intervertebral disc issues [7].

As the intervertebral disc has been demonstrated as one of the principal causes of LBP, especial interest on its structure, composition and behaviour has been stablished in order to know what causes spine diseases and issues. An intervertebral disc is formed by the nucleus pulposus, the annulus fibrosus and the cartilaginous endplates (Fig.1), and any of this components could be injured in a degenerated intervertebral disc leading to a sclerosis [8], loss of intervertebral height [9] or an irregular spine stress distribution [8] [9]. In particular, the nucleus pulposus is composed of a viscoelastic proteoglycan that cushions the pressure applied vertically to the spine regulating the height of the intervertebral disc due to its water absorption [5], but it shows the most considerable impact in the degenerating process [9] having a decrease of proteoglycan content and viscoelasticity [10] resulting in a loss of water absorption and a loss of intervertebral disc height [11]. This water loss transfers the stress concentration from the nucleus pulposus to the annulus [12] which can also present changes in its properties due to the loss of water [10] and also in flexion it leads to a massive load in vertebrae [13].

As it was explained in the previous study, the Final Degree Thesis, it was hypothesized that LBP can be explained as a loss of intervertebral disc height due to the vertebral foramen (Fig. 1, E) size reduction that squeezes the spinal nerve that passes through it. Spinal nerves originate from the spinal cord in the posterior part of the spine, and it can be damaged if the space between adjacent vertebrae (intervertebral foramen) is reduced, producing LBP [14].

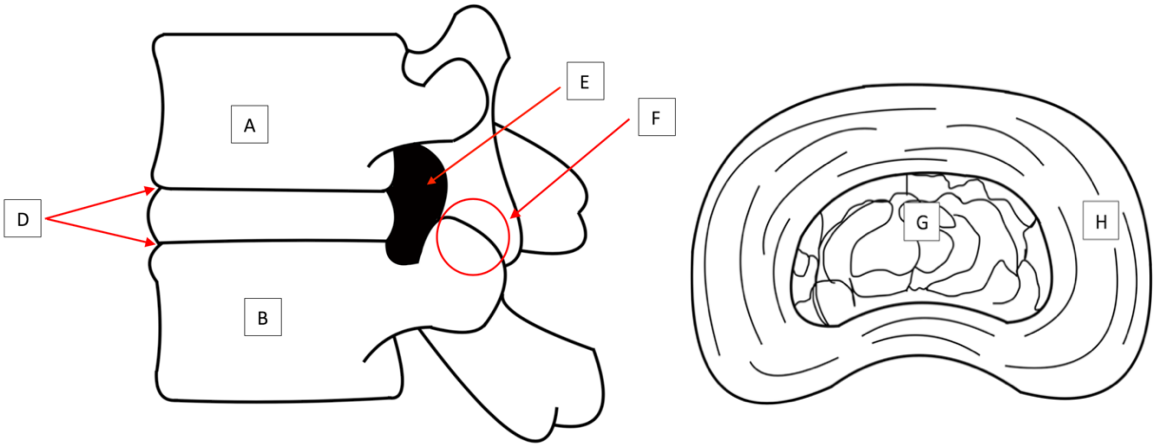

Figure 1. Representation of a 2-level vertebra segment in the lateral view (left) and an intervertebral disc in the axial view (right). A: Upper vertebra; B: Lower vertebra; C: Intervertebral disc; D: Cartilaginous endplates; E: Vertebral foramen; F: Facet joint; G: Nucleus pulposus; H: Annulus fibrosus.

1.2. Spine degeneration studies

The study of the behaviour of the spine has been challenging in order to understand the dynamic and static conditions and mechanisms responsible of the LBP disease in order to provide an effective treatment for the patient. Some of these challenges aboard in vivo studies through intradiscal transducers across the intervertebral disc [12], [13], [15], [16], [17], [18], in order to measure the strains and displacements allowing the characterization of biological tissues and their interactions with biological devices [19] (Fig. 2).

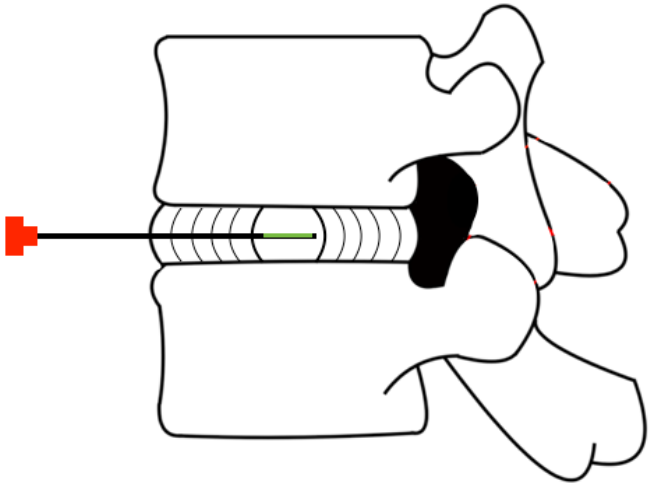

Figure 2. Representation of an intradiscal transducer test across an intervertebral disc, where at the end of the needle there is a deformable membrane (green) sensible to the pressure applied in the disc.

However, studying a living body requires to be a minimally invasive surgery in order to be safe and painless to patients during the tests, and this limits the range of possible procedures and the number of subjects of study. An alternative for this limitation is to investigate on surrogates, in particular in-vitro cadaveric specimens, to develop reliable clinical methods for patients.

In the Final Degree Thesis, spines were removed from porcine cadavers in order to find modern alternatives that can reproduce an injured patient condition in the most similar way possible, avoiding suffering of living beings and the lack of human cadavers for testing. Animal specimens are compatible alternatives to human models due to their efficiency and similarities [8], [20]. Due to that, this Final Master's Degree Thesis will carry on the previous study, basing on the materials and methods that were used there (Fig. 3).

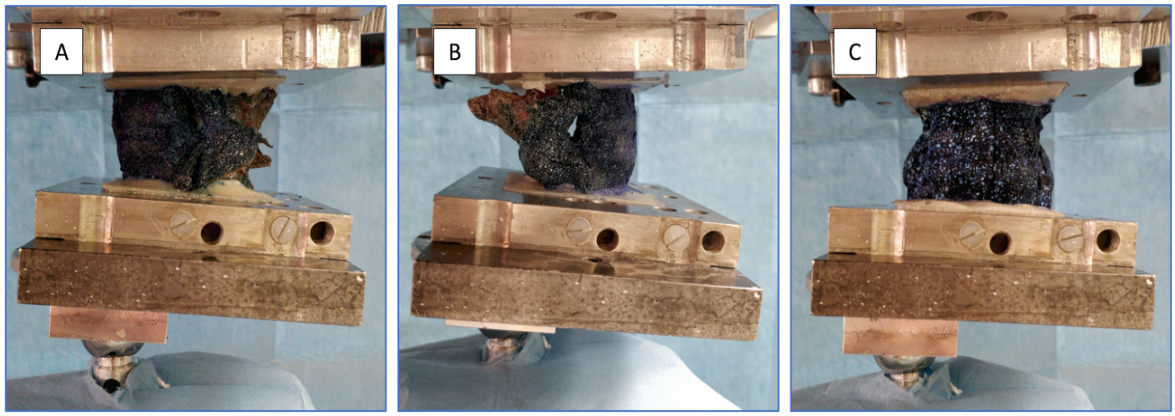

Figure 3. Ex-vivo loading test applied to an L3-L4 segment carried out in the experimental study in order to replicate the human motions. A: Flexion; B: Extension; C: Lateral bending.

1.3. Clinical surgeries and solutions

Total disc replacement has been accepted as a solution for spine degeneration for years [21]. However, further experimentations are needed due to its limited information about this field of study [22] and also its highly-invasive surgical method that needs special care and attention due to its risks that are carried out.

On the other hand, the use of biomaterials in degenerated spine tissues shows effective results used as reparation or substitution of a degenerated intervertebral disc. Some of the biomaterials that are implemented are hydrogels used as nucleus pulposus and annulus fibrosus fissures sealants [9]. Another promising alternative is the tissue engineering, that consists of cell-based therapies cultivated and injected in the spine in order to replace the injured intervertebral disc cells [23]. These tissue-engineered therapies are still growing and being developed to reduce the intervertebral disc injury by stabilizing stress and strain distribution disorders [24].

In the previous study, it was implemented and studied an application based on a percutaneous cement discoplasty (PCD), that consisted of a cement injection based on polymethyl methacrylate (PMMA) mixture in the degenerated intervertebral disc through a lateral incision in the annulus fibrosus in order to improve the stabilization, mobility and intervertebral disc height of an unhealthy spine (Figs. 4-5). This non-invasive surgical method has been implemented in other in-vitro studies injecting PMMA in the posterior part of the spine, having as a result a gain of stability, spine deviation reduction and less pain and disability. The PMMA cementation fills the hollowed intervertebral disc and distributes the load in the endplates [25], [26].

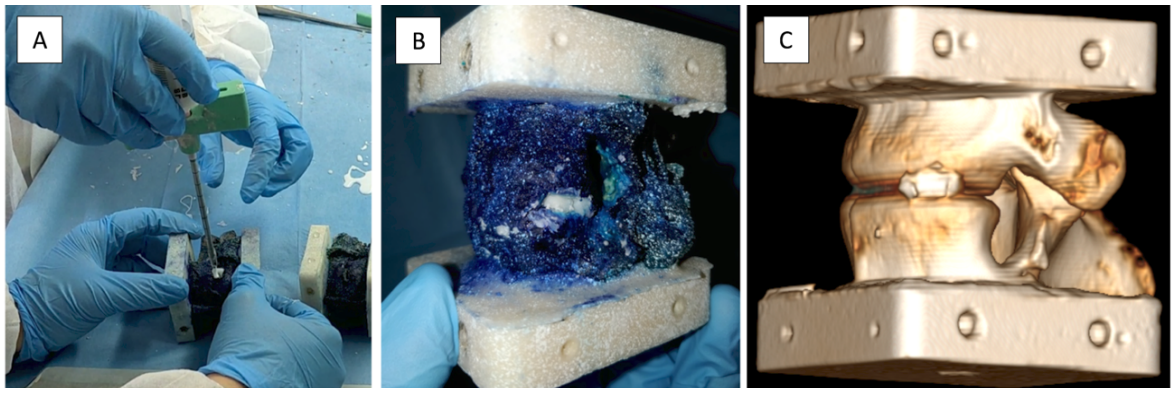

Figure 4. PCD method carried out in the Final Degree Thesis. A: Injection of the cement in the puncture while the specimen is manually positioned in tension; B: Result of the cementation; C: Specimen micro-CT reconstruction.

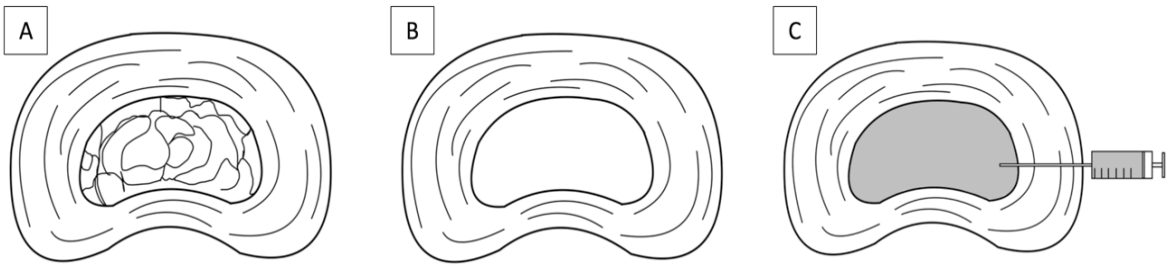

Figure 5. Schematic representation of the PCD. A: Healthy/intact nucleus pulposus; B: Unhealthy/degenerated nucleus pulposus; C: PMMA cemented nucleus pulposus.

In the Final Degree Thesis, it was concluded that the PCD method using PMMA for filling the empty nucleus pulposus recovers the intervertebral disc height and stability lost in a degenerated disc without compromising the spine motion.

1.4. From Digital Imagen Correlation (DIC) to Finite Element Method (FEM)

In the Final Degree Thesis, the Digital Image Correlation (DIC) was used in order to study the behaviour of the spine. It consisted of a non-invasive measurement method that records the full-field of displacements and strains [27].

The DIC had his first appearance in micro and nanomechanical testing in the early 70' [28]. In the late 90', it was applied in biomechanical testing [29], giving the subject-specific response from a specific part of a immobilized body imposed to a motion that replicates the biomechanics of the human being and registering the distribution of deformations in the surface with accuracy and precision [30]. The correlation is performed using multiple images giving a 3D representation of the sample [19] (Fig. 6).

Likewise, the Digital Volume Correlation (DVC) allows measuring the strain distribution also inside the vertebra, but it is affected by the time-consuming image acquisition, being required to scan the specimen previously with micro-CT to evaluate the reliability of DVC [31].

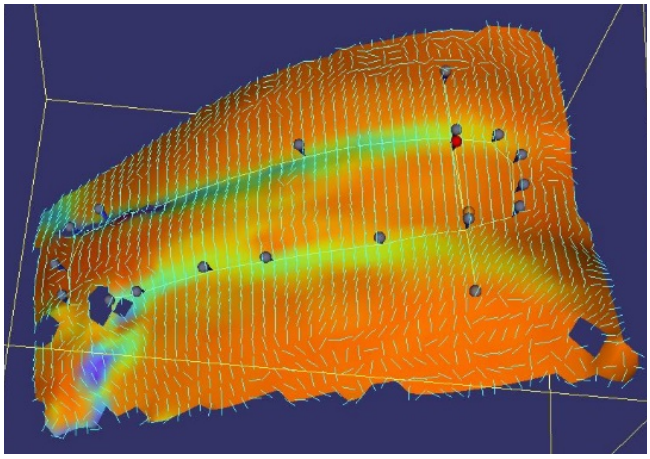

Figure 6. DIC strain representation in a L3-L4 specimen surface from the Final Degree Thesis through the Istra-4D software (Dantec Dynamics) specifically designed for DIC applications. It is observed the endplates delimited by the strain concentrations.

Some authors have studied the biomechanical behaviour of the spine using the Finite Element Method (FEM) consisting of defining the geometry and material properties from a previously scanned spine by Computed Tomography (CT) [32] or also it can be modelled and simulated by computer [33], [34], [35]. Some of the advantages of this procedure compared with the DIC method are:

- Savings in costs for materials of subjects, machinery and facilities: in the previous study, 11 pig lumbar spine segments composed of the intervertebral disc between 2 vertebrae that needed freezers for their maintenance were used. They were tested in a servo-hydraulic universal loading machine (8032, Instron, High Wycombe, UK).

- Faster specimen preparation: the DIC method required to be obtained ethically from cadaveric pigs, an aligned and fixed PMMA cementation for the loading machine, a specific dye for the correlation optimization, a preparation for each specimen for simulating the degeneration and cemented conditions through an incision in the annulus fibrosus, a sensible calibration of the DIC cameras and a freeze of the specimens in order to preserve their functional, structural and biological properties.
- Reproducibility of data: in FEM simulations, the results are reproducible without depending on environmental conditions as the DIC method, that required 11 different specimens and the tests were repeated twice to achieve the reproducibility of the dataset.
- Accurate data collection: the FEM simulations obtain a complete map of the strain distribution in the whole model (as in the DVC method) and also it can be specifically selected depending on the desired component of the vertebrae.

However, FEM models are usually simplified regarding the constitutive model, the biomechanical properties and the shapes of each vertebrae component due to limitations of the software that simulates the test or the difficulty to achieve the convergence of the solution. The synergy between simplifications, assumptions, material properties, shapes, test inputs and outputs will explain experimental results, but their predictive ability is limited to independent predictions [20].

This work will be carried out using CT models obtained from the PMMA cemented specimens from the previous study (Fig. 7) in order to analyse through the FEM method, the strain and displacement distribution under similar conditions to those applied in the DIC method.

Figure 7. DICOM images of L3-L4 PMMA cemented specimen CT scanned. A: Axial view; B: Sagittal view; C: Coronal view.

1.5. Objective of the study

Starting from the materials and methods of the previous study, a FEM model of a L3-L4 porcine segment was developed in order to simulate the loading conditions during the DIC recording in flexion, extension and lateral bending. The models obtained replicated the healthy, degenerated and PMMA cemented conditions, and also distinguishing the incision and the intact removal from the degenerated and the PMMA cemented ones in order to study the influence of the incision that was performed in the annulus fibrosus for the removal of the nucleus pulposus and the posterior PMMA injection. Therefore, there were 5 models under study whose geometry was obtained from the same CT images.

The main objective of the study is to carry out the DIC study using the FEM analysis in order to achieve reliable results and to avoid animal testing and saving costs of testing.

2. MATERIALS AND METHODS

2.1. Segmentation of the specimen

As it has been explained before, the model for the FEM simulation was obtained from DICOM images of a CT scanning (Fig. 7). The scanned specimen was a L3-L4 segment that was potted with a PMMA cementation and also with the nucleus pulposus PMMA cemented (Fig. 8).

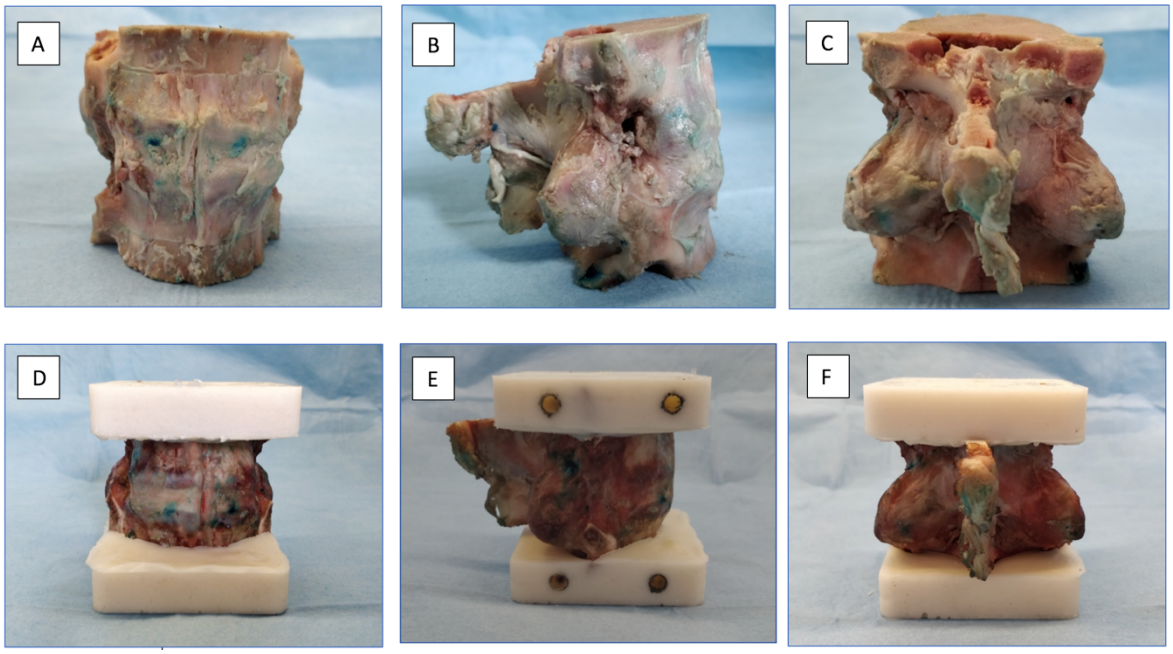

Figure 8. L3-L4 spine segment after soft tissue cleaning and PMMA cementation in both extremities. A, D: Anterior view; B, E: Lateral view; C, F: Posterior view.

2.1.1. Healthy and PMMA-cemented models

Through the free and open source software 3DSlicer, the CT structure was obtained and displayed in order to perform a model that replicates the dimensions and shapes of the parts of interest of the specimen (Fig. 9). The model was obtained through the threshold, cutter and smoothing tools in order to preserve the bone and providing a smooth surface for a simplification of the model (Fig. 10). It was eliminated the ligaments and soft tissues of the specimen and the PMMA pot.

The same 3DSlicer segmentation was used for both healthy and PMMA cemented models in order to assign the materials (both nucleus pulposus and PMMA respectively) for the simulation.

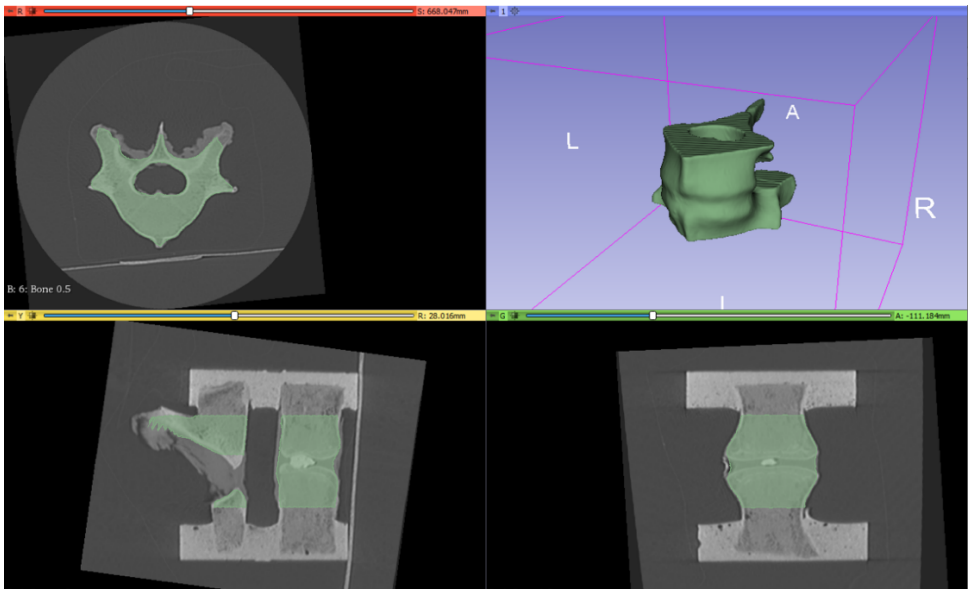

Figure 9. 3DSlicer segmentation of the specimen. Green: Segmentation of the CT.

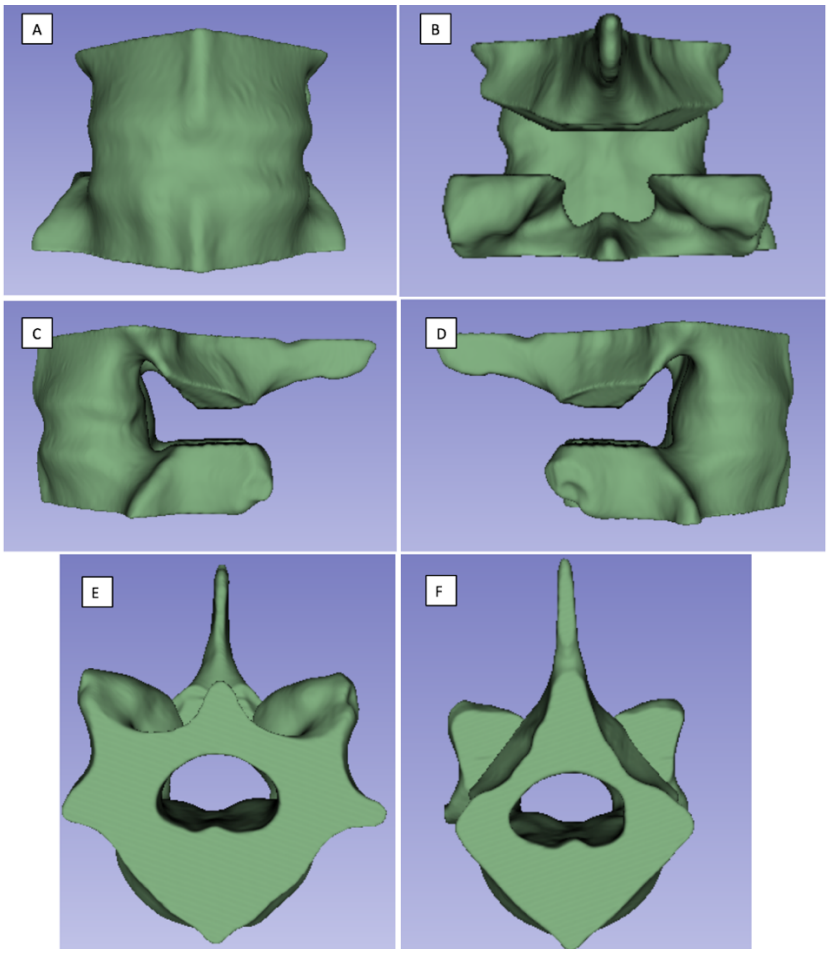

Figure 10. Healthy and PMMA-cemented model created of the L3-L4 spine segment through the 3DSlicer. A: Anterior view; B: Posterior view; C: Right view; D: Left view; E: Lower view; F: Upper view.

2.1.2. Degenerated models

As for the degenerated model, it consisted of an intervertebral disc without nucleus pulposus. It was recreated removing the PMMA cemented part of the CT image since the nucleus pulposus of the specimen was fulfilled with the cementation (Fig. 11).

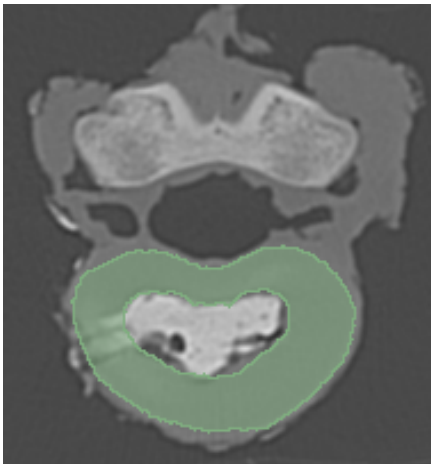

Figure 11. Axial representation of the nucleus pulposus removal through the segmentation in 3DSlicer. It is shown that the nucleus pulposus is not selected in the segmentation.

This degenerated model (Fig. 11) is the ideal state of a degenerated intervertebral disc. However, in the previous study, it was necessary to remove the nucleus pulposus of the specimen by manually extracting the nucleus. The procedure consisted of reaching the nucleus digging into the annulus fibrosus using a scalpel (Fig. 12). A hole of about 5 x 5 mm was performed in order to remove the nucleus pulposus.

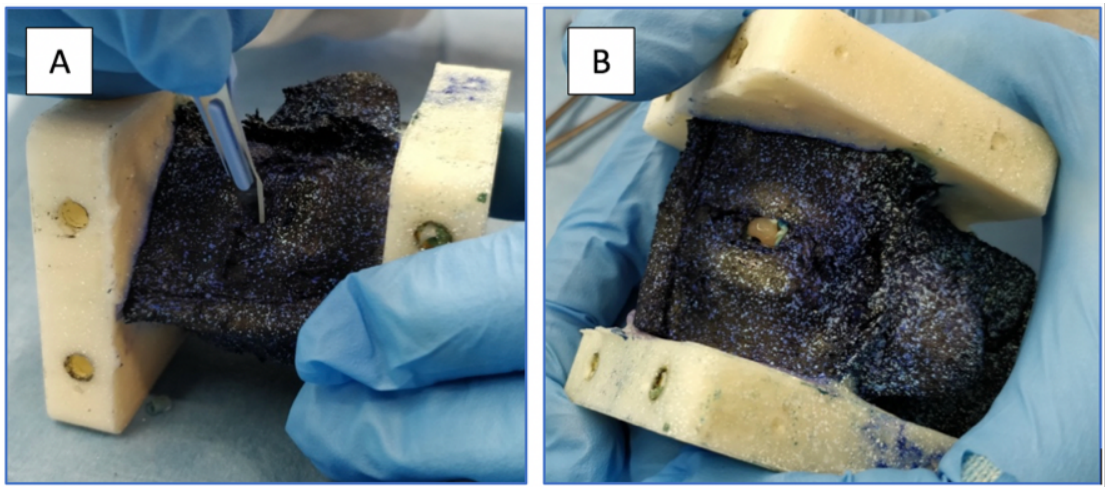

Figure 12. Nucleus pulposus removal procedure in the experimental study. A: With a scalpel, it is made a puncture in the annulus fibrosus in the opposite side of the region of interest of the specimen; B: The nucleus pulposus comes out of the puncture when is applied a compression.

In order to replicate the incision, it was removed the PMMA cementation that remained in the incision part of the annulus fibrosus observable in the CT (Fig. 13), resulting on a longitudinal hole in the left side of the model (Fig. 14)

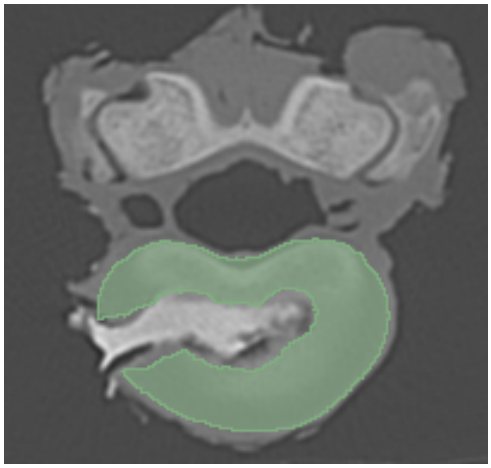

Figure 13. Axial representation of the nucleus pulposus removal and incision through the segmentation in 3DSlicer.

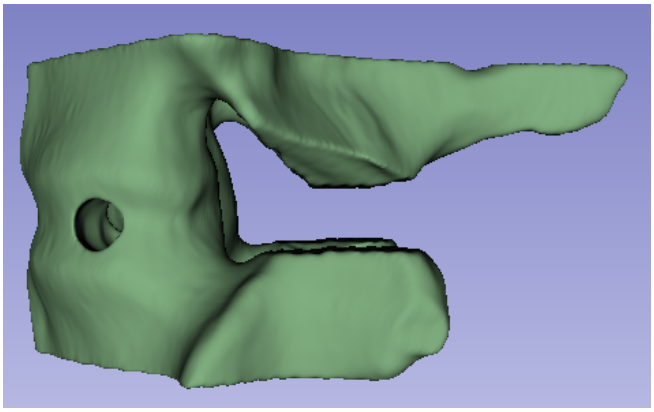

Figure 14. Result of the incision in the left side of the healthy model (degenerated-incision model).

2.2. Incision and non-incision models

The degenerated and PMMA models with an incision are based on the degenerated and PMMA-cemented specimens that were tested in the experimental study. These models are differentiated from the degenerated and PMMA cemented models without incision in order to answer a crucial question derived in the previous study about the effect of doing an incision on the annulus fibrosus for the rotation of the lower vertebra, the strain distribution and overall structural behaviour of the remaining disc.

Therefore, in this study there were tested 5 different models in order to compare different results and achieve different objectives:

- Healthy/intact model.
- Unhealthy/degenerated model.
- Unhealthy/degenerated model with incision (degenerated-incision model).
- PMMA-cemented model.
- PMMA-cemented model with incision (PMMA-incision model).

2.3. Finding the optimal model mesh parameters

Through a custom-made Matlab code (Appendix I), the models were meshed with different element sizes in order to achieve the optimal mesh parameters. The assignment of each part or the vertebrae for every model (upper vertebra, annulus fibrosus, nucleus pulposus, PMMA and lower vertebra) was manually selected from CT visualization (Figs. 15-16). It was observed that the number of elements and the accuracy of the part selection decreases drastically with high element sizes.

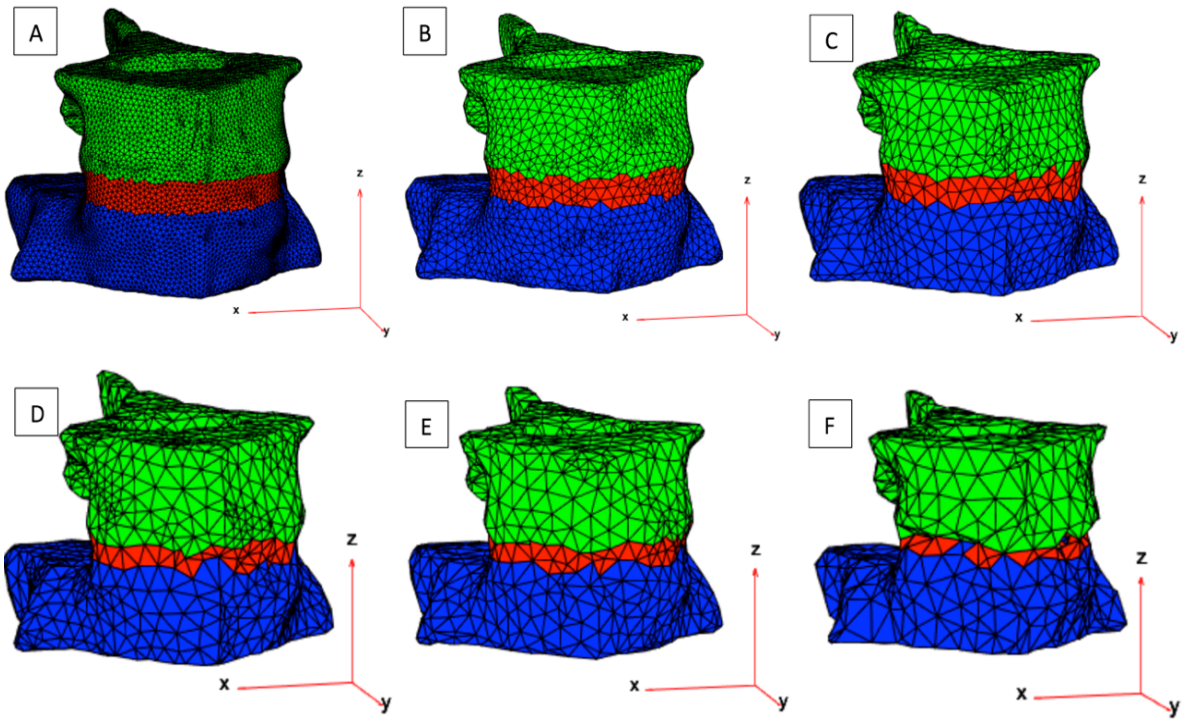

Figure 15. Overall representation of the model with different mesh sizes. Green: Upper vertebra; Red: Annulus fibrosus; Blue: Lower vertebra; A to F: Increasing element size.

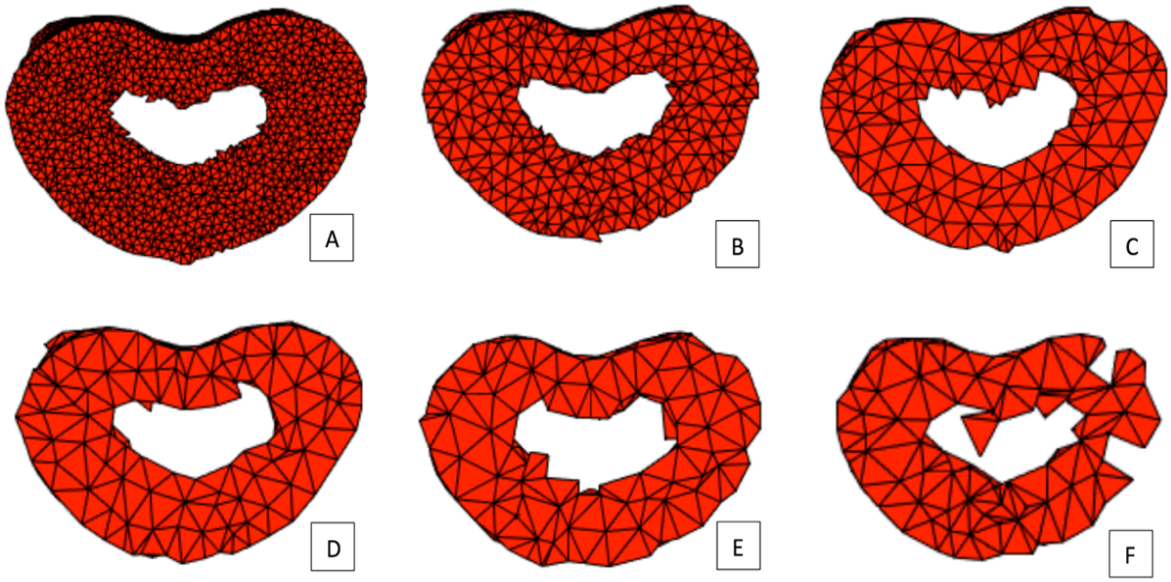

Figure 16. Axial representation of the degenerated intervertebral disc from a posterior view. for different element sizes. As it is shown, it is just represented as a annulus fibrosus element without nucleus pulposus. A to F: Increasing element size.

The software in which simulations were performed, ANSYS APDL Academic (ANSYS, Inc.), has a limit of 32.000 nodes/elements for structural analyses, being the A and B element sizes shown in Figure 15 non-viable for the analysis because of the limit exceed. Therefore, the selected element size for the simulation was of a size between the B and C element size.

2.4. Material definitions

As for the material properties selected for each model, a linear elastic behavior was assumed for all the materials. Therefore, two mechanical properties were used in order to simulate the loading test:

- The Young modulus (E), that measures the stiffness of a material from the relationship between the stress and the strain when a uniaxial elastic load is applied in the material.
- The Poisson's ratio (υ), that measures the expansion and contraction of a material perpendicular to the loading direction.

Thus, using the same code mentioned previously, the following values were assigned to the materials used in this study based on the literature and research from other authors:

- Upper and lower bone: each part was considered as a cortical bone for simplification.
  - E = 12.000 MPa [36], [37].
  - υ = 0,3 [36], [37].

- Annulus fibrosus:
  - E = 450 MPa [38].
  - υ = 0,3 [38].
- Nucleus pulposus:
  - E = 1 MPa [36], [39].
  - υ = 0,49 [36].
- PMMA: these values were obtained by Bouziane et al. through a FEM analysis of a PMMA-based hip spacer.
  - E = 2.700 MPa [40].
  - υ = 0,35 [40].

Thus, the final models prepared for the FEM analysis through ANSYS APDL were:

1. Healthy model (Fig. 17):
   - 6.058 nodes.
   - 26.161 elements.
   - Model generation in 138 seconds.

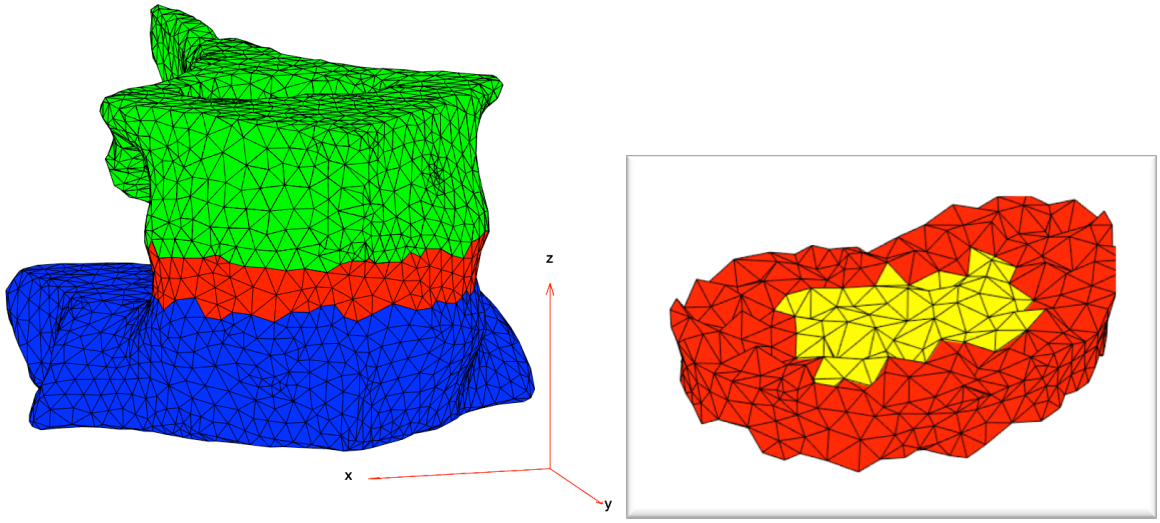

Figure 17. Healthy model (left) and its intervertebral disc (right). Green: Upper vertebra; Blue: Lower vertebra; Red: Annulus fibrosus; Yellow: Nucleus pulposus.

2. Degenerated model (Fig. 18):
   - 5.856 nodes.
   - 25.025 elements.
   - Model generation in 154 seconds.

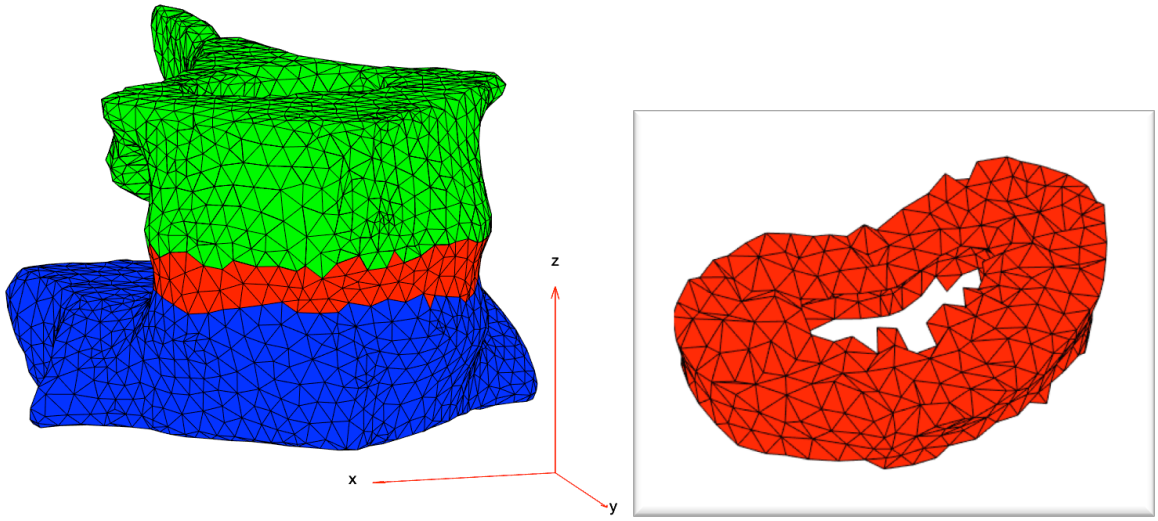

Figure 18. Degenerated model (left) and its intervertebral disc (right). Green: Upper vertebra; Blue: Lower vertebra; Red: Annulus fibrosus.

3. Degenerated-incision model (Fig. 19):
    - 5.986 nodes.
    - 25.494 elements.
    - Model generation in 141 seconds.

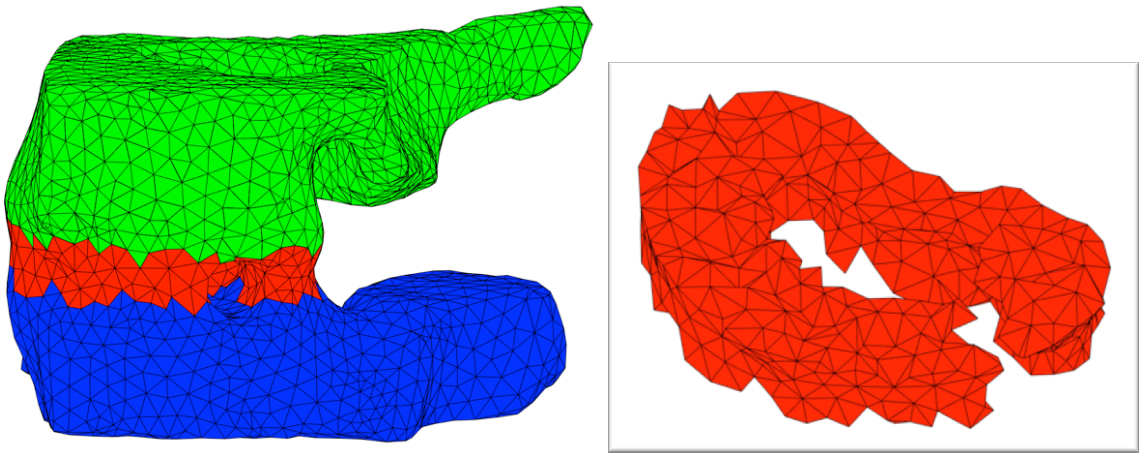

Figure 19. Degenerated-incision model (left) and its intervertebral disc (right). Green: Upper vertebra; Blue: Lower vertebra; Red: Annulus fibrosus.

4. PMMA-cemented model (Fig. 20):
    - 6.058 nodes.
    - 26.161 elements.
    - Model generation in 140 seconds.

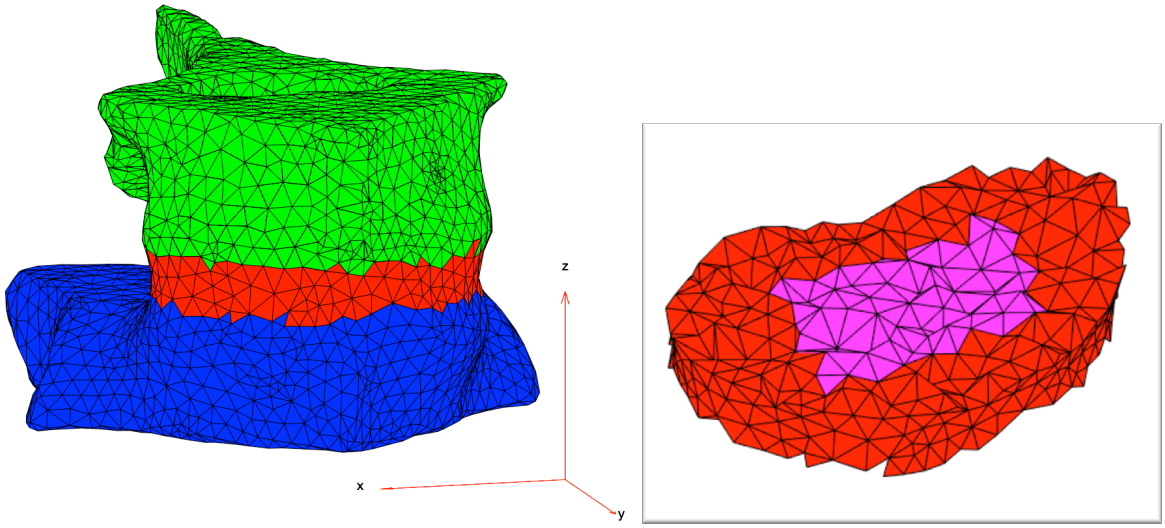

Figure 20. PMMA-cemented model (left) and its intervertebral disc (right). Green: Upper vertebra; Blue: Lower vertebra; Red: Annulus fibrosus; Magenta: PMMA.

5. PMMA-incision-cemented model (Fig. 21):
    - 6.058 nodes.
    - 26.161 elements.
    - Model generation in 140 seconds.

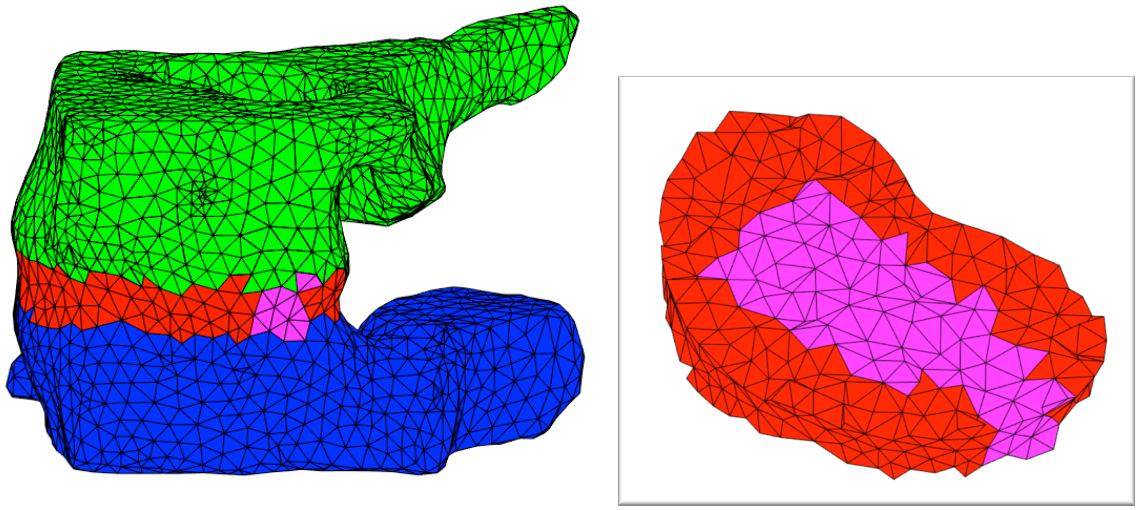

Figure 21. PMMA-incision-cemented model (left) and its intervertebral disc (right). Green: Upper vertebra; Blue: Lower vertebra; Red: Annulus fibrosus; Magenta: PMMA.

2.5. Simulation

As it was explained before, the simulations were performed through the software ANSYS APDL Academic, where it was imported and displayed the ".ans" files that contained the information about the node coordinates, mesh elements and the properties of the materials generated through the previous custom-made MATLAB code for each model (Fig. 22).

There were 5 models in total (healthy, degenerated, degenerated-incision, PMMA, and PMMA-incision). A flexion, an extension, and a lateral bending were simulated for each one of them, as it was physically performed in the Final Degree Thesis.

Thus, 15 tests in total (3 tests for each one of the 5 models) were simulated. The strain distribution, the relative rotation (ROM), and the relative translation (TR) of the lower bone were registered (section 2.5.2.).

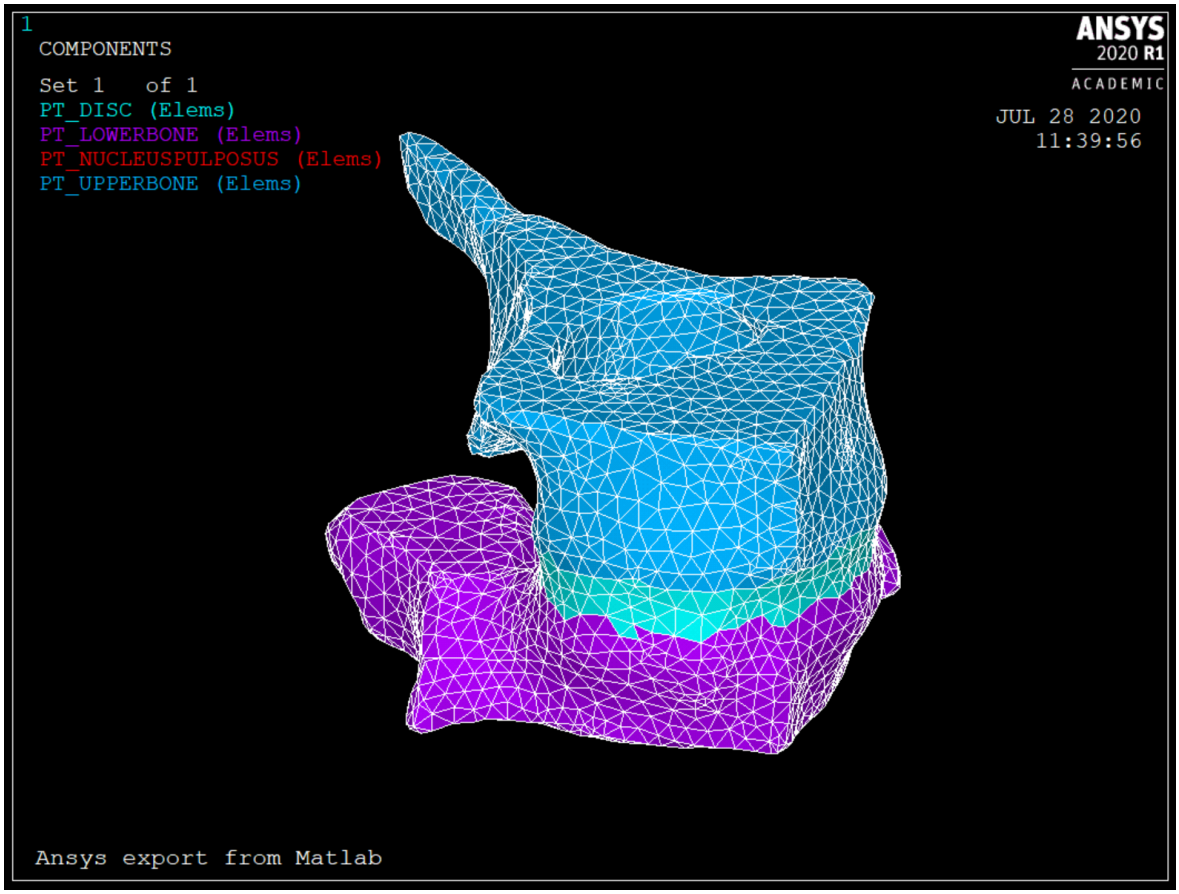

Figure 22. 2.5 mesh size healthy model displayed on the ANSYS APDL Academic software. Blue: Upper bone; Light blue: Annulus fibrosus; Purple: Lower bone.

2.5.1. Test configuration

Each simulation was performed as a test in which the upper bone was totally fixed. A single force of 100 N was applied at the lower vertebra in z-direction in order to replicate the ball and socket joint from the experimental tests (Fig. 3). The application of the displacements and forces were manually selected. Figure 23 shows a left view of the flexion test configuration, Figure 24 shows a left view of the extension test configuration, and Figure 25 shows an anterior view of the lateral bending test configuration.

In the previous study, it was carried out the pre-conditioning (consisting on 20 cycles of 200 N at 50 Hz before the loading test), 6 loading cycles at 200 N (equivalent to 5,4 Nm) and the repetition of the simulation. In this study, these aspects were omitted because of the model simplification and the previous specimens were freeze and needed the pre-conditioning for its preparation.

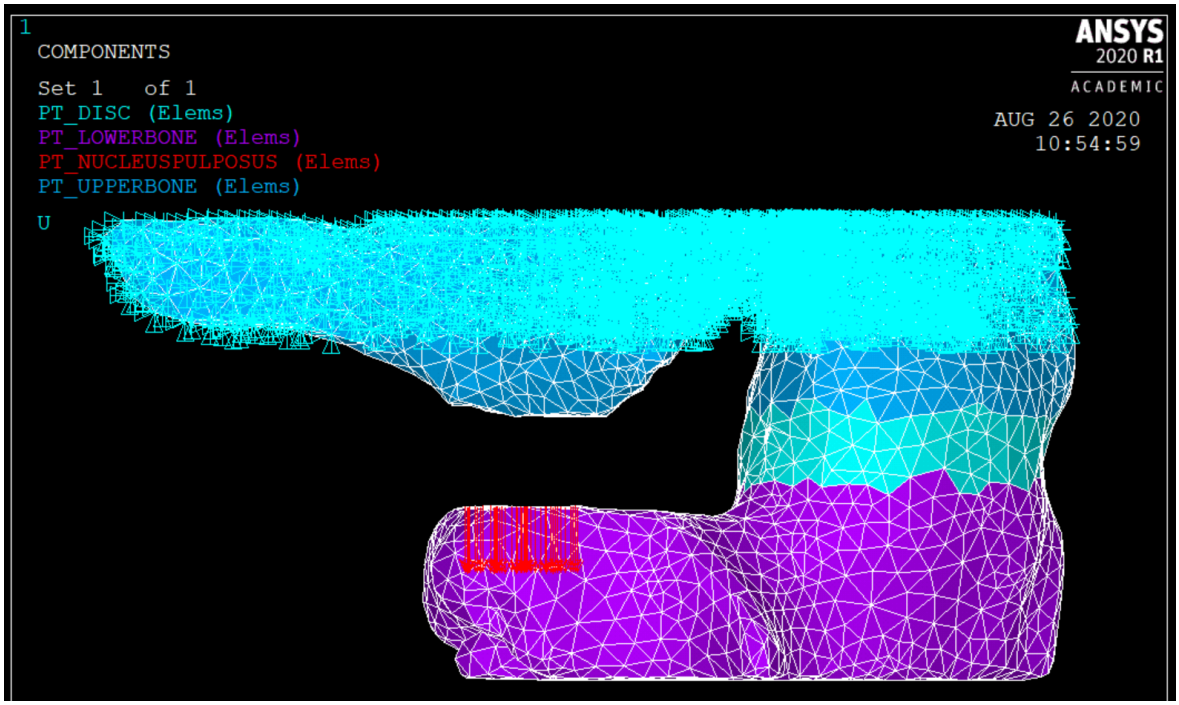

Figure 23. Left view of the representation of the flexion test configuration. Blue triangles: Displacement restriction; Red arrows: Force applied on the Z-axis direction.

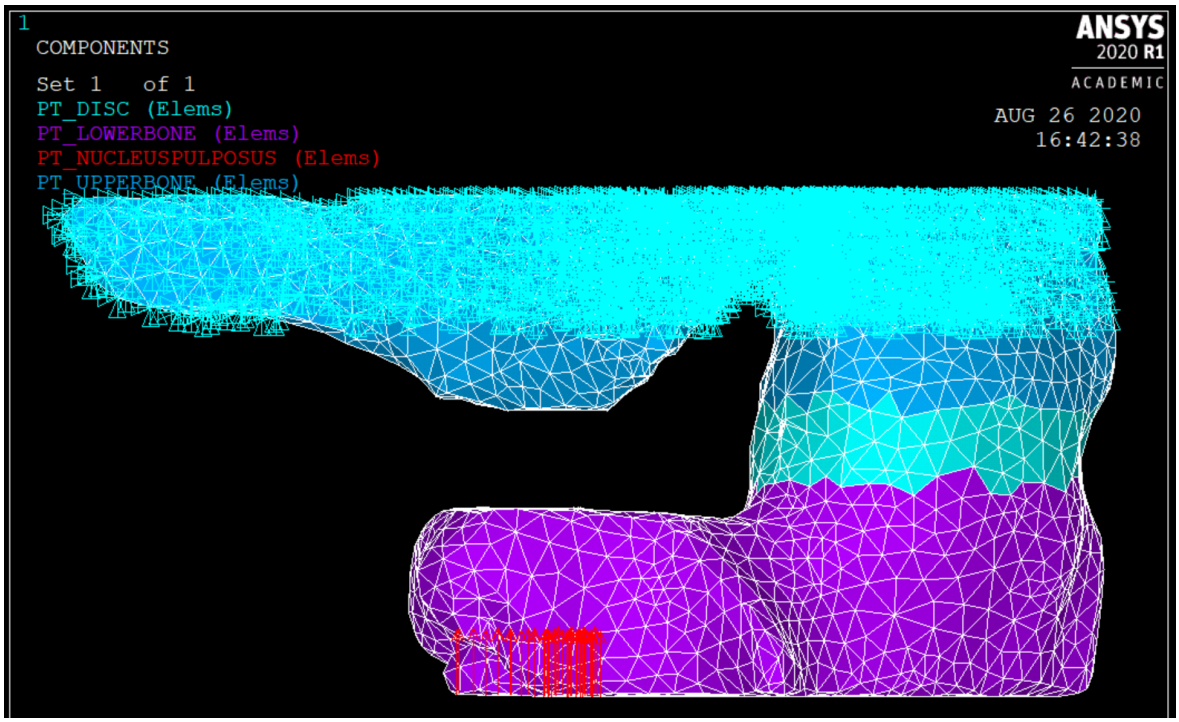

Figure 24. Left view of the representation of the extension test configuration. Blue triangles: Displacement restriction; Red arrows: Force applied on the Z-axis direction.

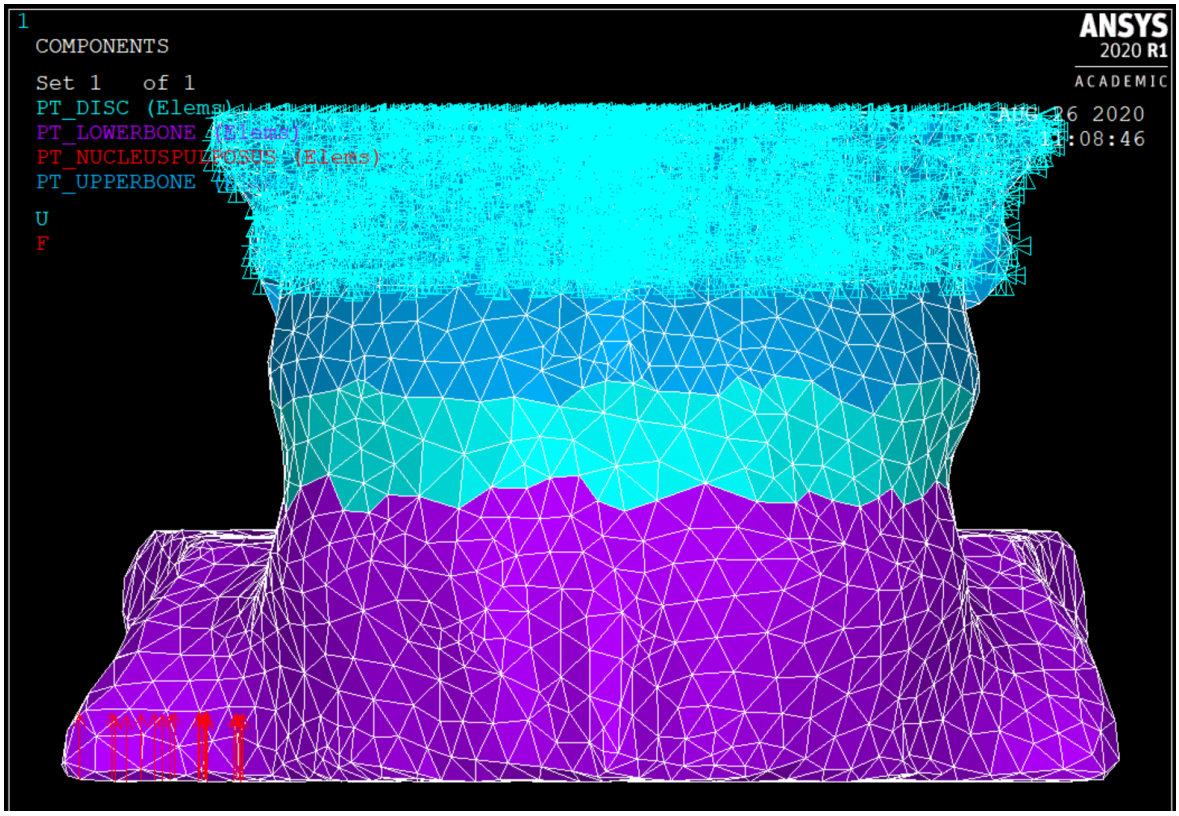

Figure 25. Anterior view of the representation of the lateral bending test configuration. Blue triangles: Displacement restriction; Red arrows: Force applied on the Z-axis direction.

2.5.2. Test outputs

As it was explained before, there were 15 tests in total, from which the following data outputs were studied:

- Relative rotation (ROM): rotation of the lower vertebra compared with the upper vertebra.
- Relative translation (TR): movement of the lower vertebra compared with the initial position.
- Strain: maximum and minimum strain values in the intervertebral disc. The Region of Interest (ROI) was located on the anterior and right views of the intervertebral disc, being ignored the bone and the posterior and left view of the disc in which it was located the incision part.

In the experimental study, the results from the disc height, the viscosity and the micromotion of the upper bone were obtained. However, non-statistical differences were obtained except for the intervertebral disc height, for which the increase of height after the PMMA cementation of the disc had already been proved.

2.5.2.1. Relative rotation (ROM)

Once the tests were carried out, the nodal displacements were exported in order to obtain the relative rotation of the lower bone (Fig. 26).

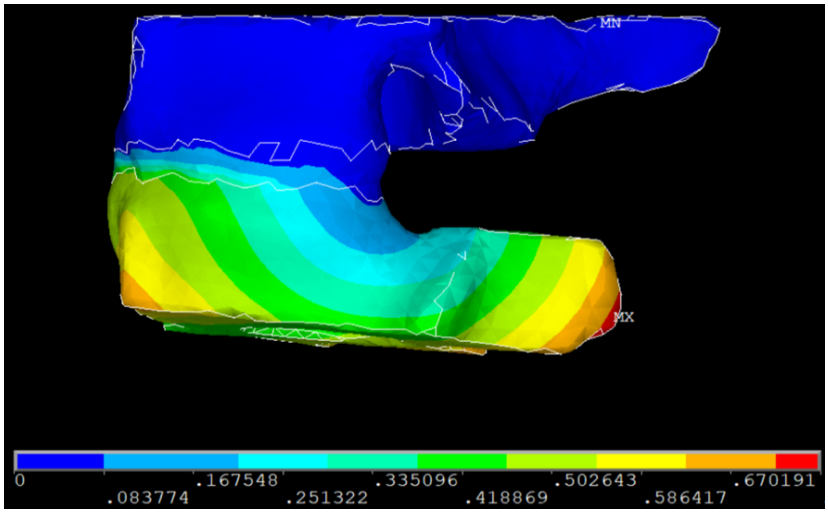

Figure 26. Representation of the rotation after a flexion motion in a healthy model.

The ROM of the lower vertebra was obtained using another custom-made MATLAB code (Appendix II) that consisted of measuring the angles that formed the vectors that join the centroids of both vertebras by calculating the cosine that these vectors formed (Fig. 27) using the equation:

$$\cos\alpha = \frac{\overrightarrow{G1G2} \cdot \overrightarrow{G'1G'2}}{|\overrightarrow{G1G2}| \cdot |\overrightarrow{G'1G'2}|}$$

where G1 and G2 are the centroids of the upper and lower vertebra respectively and G' stands for the centroids after the motion.

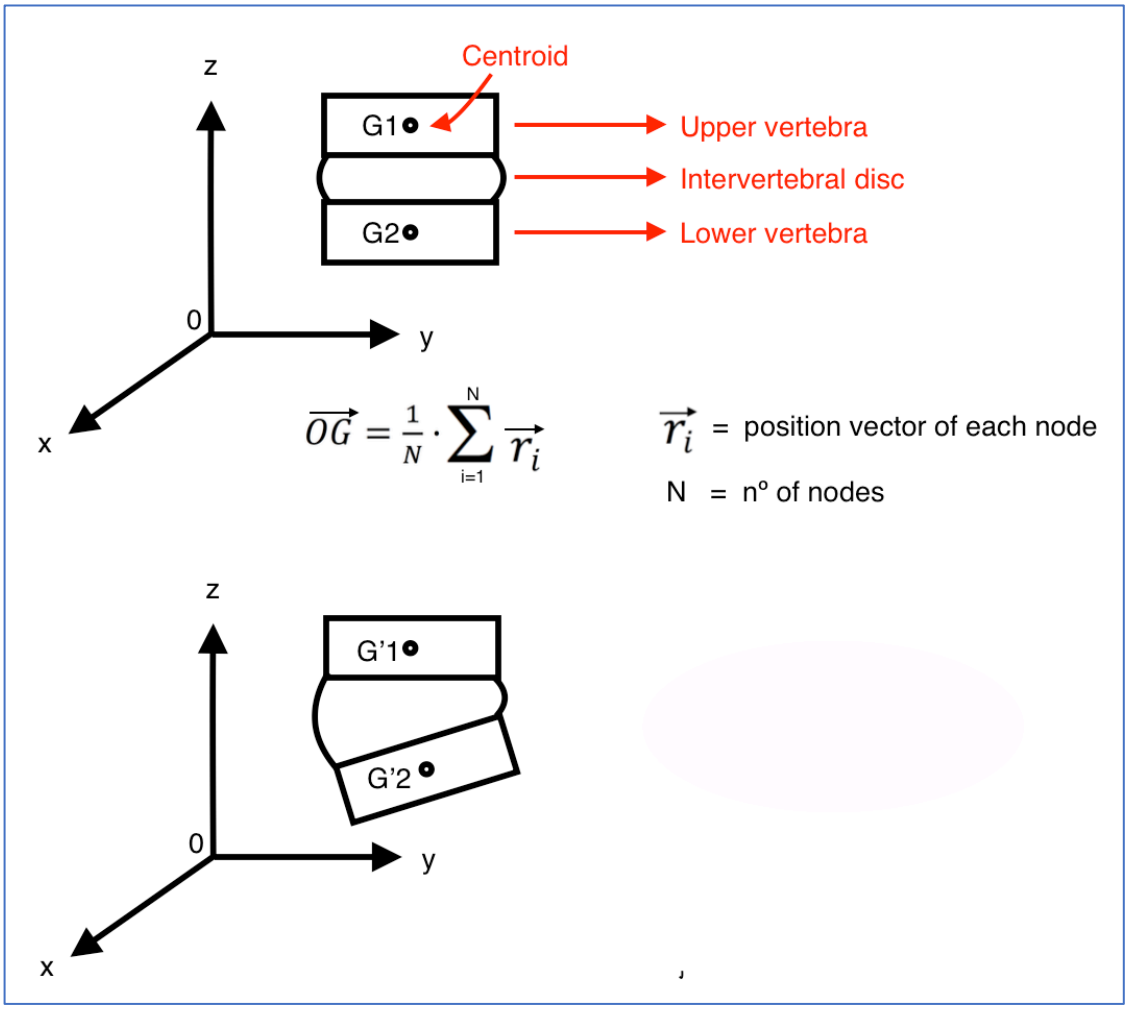

Figure 27. Representation of the angle calculation for every motion.

2.5.2.2. Relative translation (TR)

For the relative translation, using the same MATLAB code for ROM calculation, the coordinates of the lower centroids are calculated before and after the motion and then it is calculated the displacement along the z-axis as the absolute value of the difference between the motion of G2 (G'2) and the initial position, G2, in order to measure the vertical movement or compression that is generated.

2.5.2.3. Strains

As the experimental study, the transversal and axial strains of the intervertebral disc surface (Fig. 28) were obtained from the strain distribution of the nodal solution through ANSYS APDL Academic (Figs. 29 and 30), being the values of interest the minimum and maximum values of the intervertebral disc right-anterior surface, the ROI of the disc (Fig. 31).

The quantity "strain" is represented as a value that measures in microstrains ($\mu\varepsilon$, in the order of 10e-6). This measurement allows to understand the behaviour of the intervertebral disc: the positive (or maximum strain) is explained as the prominence or bulge of the intervertebral disc whereas minimum strain is the compression or depression of the disc.

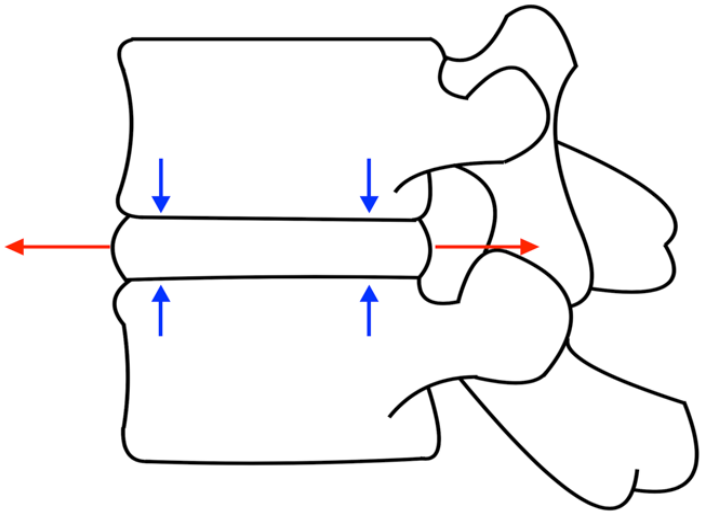

Figure 28. Representation of axial (blue) and transversal (red) strains in an anterior view.

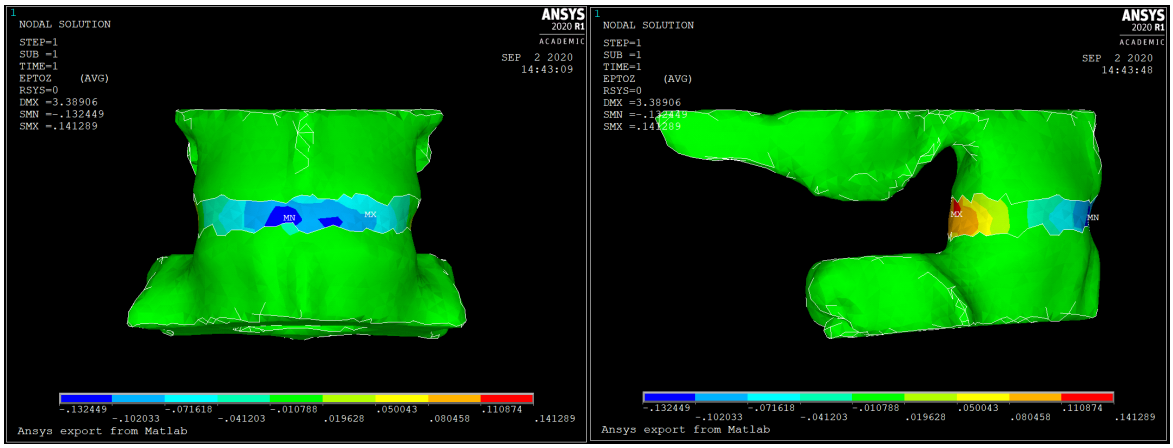

Figure 29. Representation of the axial strain of the healthy model in an example flexion test. Left: Anterior view; Right: Right view.

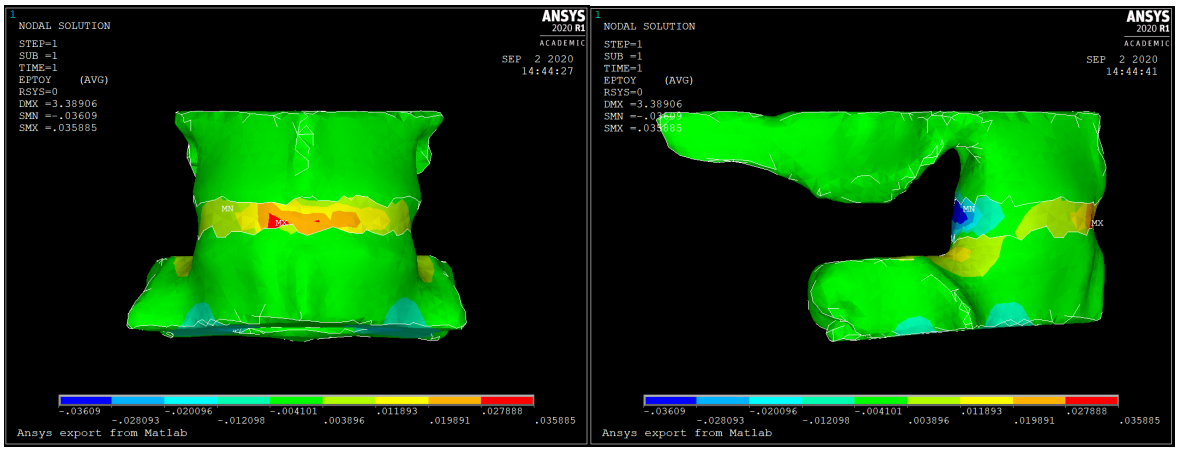

Figure 30. Representation of the transversal strain of the healthy model in an example flexion test. Left: Anterior view; Right: Right view.

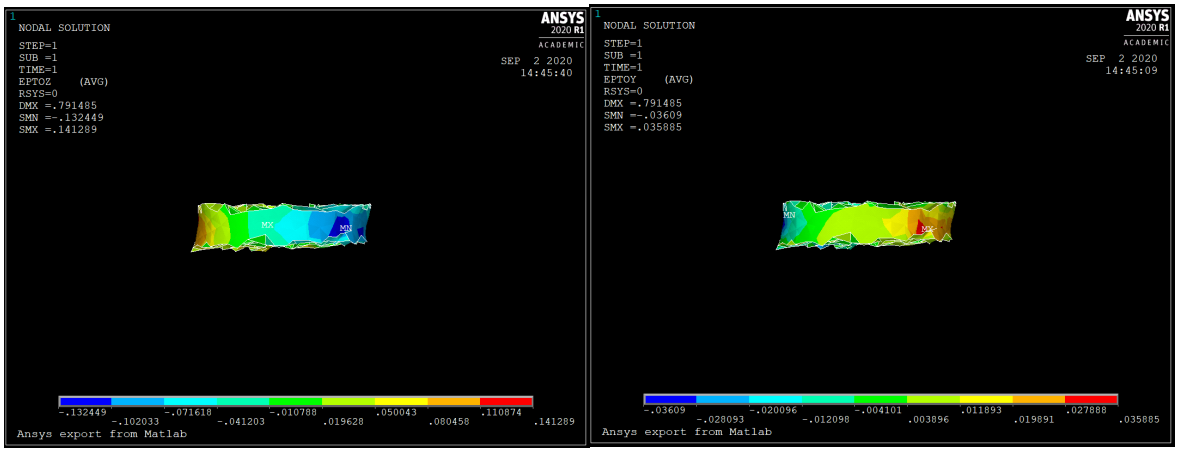

Figure 31. Representation of the axial and transversal strain distributions in the ROI of intervertebral disc of the healthy model in an example flexion test. Left: Axial; Right: Transversal.

Once recorded the maximum and minimum axial and transversal strain values, the different motions and models were compared for study the evolution of the strain distribution depending on the intervertebral disc conditions.

3. RESULTS

3.1. Relative rotation

The rotation of the lower bone in the healthy model was 1.52º, 0.93º and 0.38º for flexion, extension and lateral bending respectively (Fig. 32).

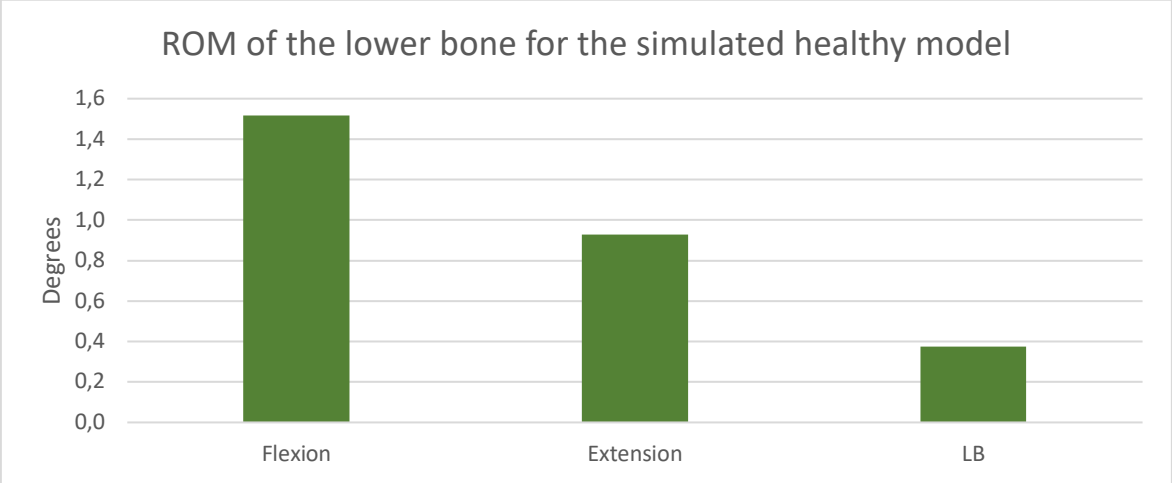

Figure 32. Lower vertebra ROM obtained from the simulation for the healthy model.

As for the comparison between the different models, Figure 33 shows a decrease of the rotation in extension and in lateral bending motions as it was shown previously for the healthy model (Fig. 32). Also, the values of the ROM for degenerated and degenerated-incision models are slightly different whereas PMMA and PMMA-incision variations have no differences in flexion but some dissimilarities in extension and lateral bending.

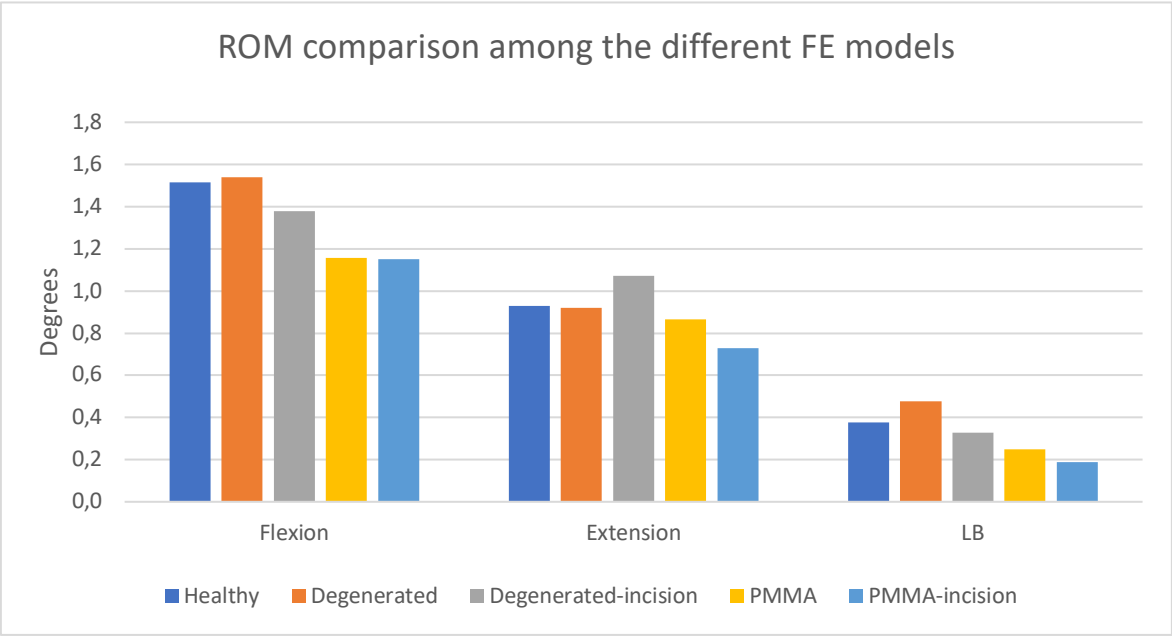

Figure 33. ROM comparison among the different FE models depending on the motion.

As for the comparison of the normalized ROMs for the degenerated models compared to the healthy model, Figure 34 shows high differences for lateral bending, having a higher increase the degenerated model (127% for the degenerated and 87% for the degenerated-incision) but more or less the same results for flexion and extension (approximately 90% and 110% for flexion and extension respectively). As for the degenerated experimental data, it is very close to the values obtained in the degenerated-incision model.

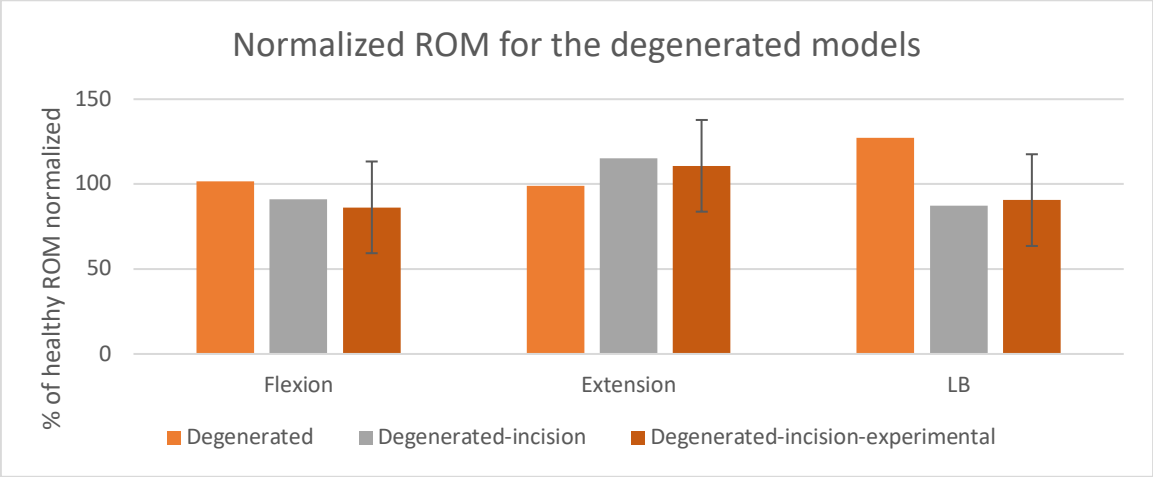

Figure 34. Normalized ROMs for the degenerated model compared to the healthy model.

On the other hand, normalized ROMs for the PMMA models have an observable ROM decrease compared to the healthy model (Fig. 35), having non-significant differences between the PMMA and the PMMA-incision models for flexion (≈ 78%) but differences for extension and lateral bending (93% and 66% for PMMA model versus 78% and 51% for PMMA-incision for extension and lateral bending respectively). The result for flexion seems to be according to the experimental data. However, the experimental results for extension and lateral bending are far from the results from the simulation since they showed a small increase in extension and lateral bending motions (108% and 104% respectively).

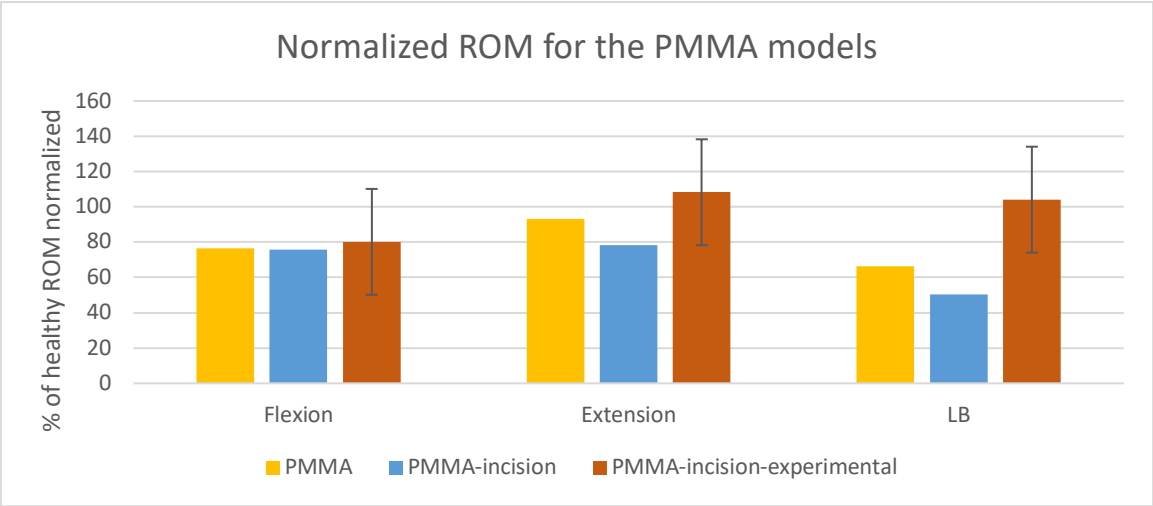

Figure 35. Normalized ROMs for the PMMA models compared to the healthy model.

3.2. Relative translation

As for the relative translation of the lower vertebra, it was obtained, for the healthy model, a movement in the z-axis (vertical direction) of 0.94mm, 3.61mm and 0.19mm for flexion (Fig. 36), extension and lateral bending, respectively.

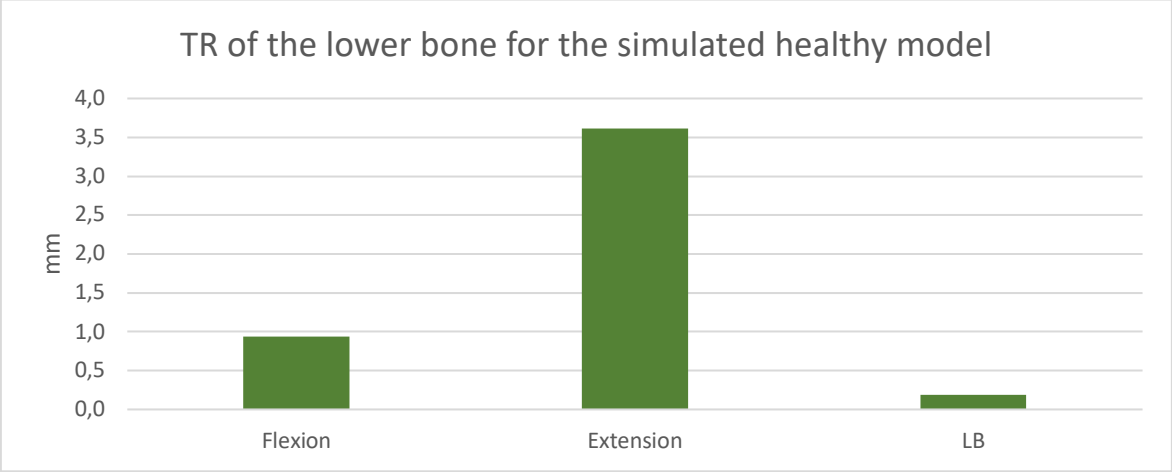

Figure 36. Lower vertebra TR obtained from the simulation for the healthy model.

Comparing the relative translations obtained for every model and every motion (Fig. 37), it was observed a trend that shows non-statistical differences among them expect for extension in the healthy model, where there is a vertical movement of 3.61mm, really out of the trend that is followed.

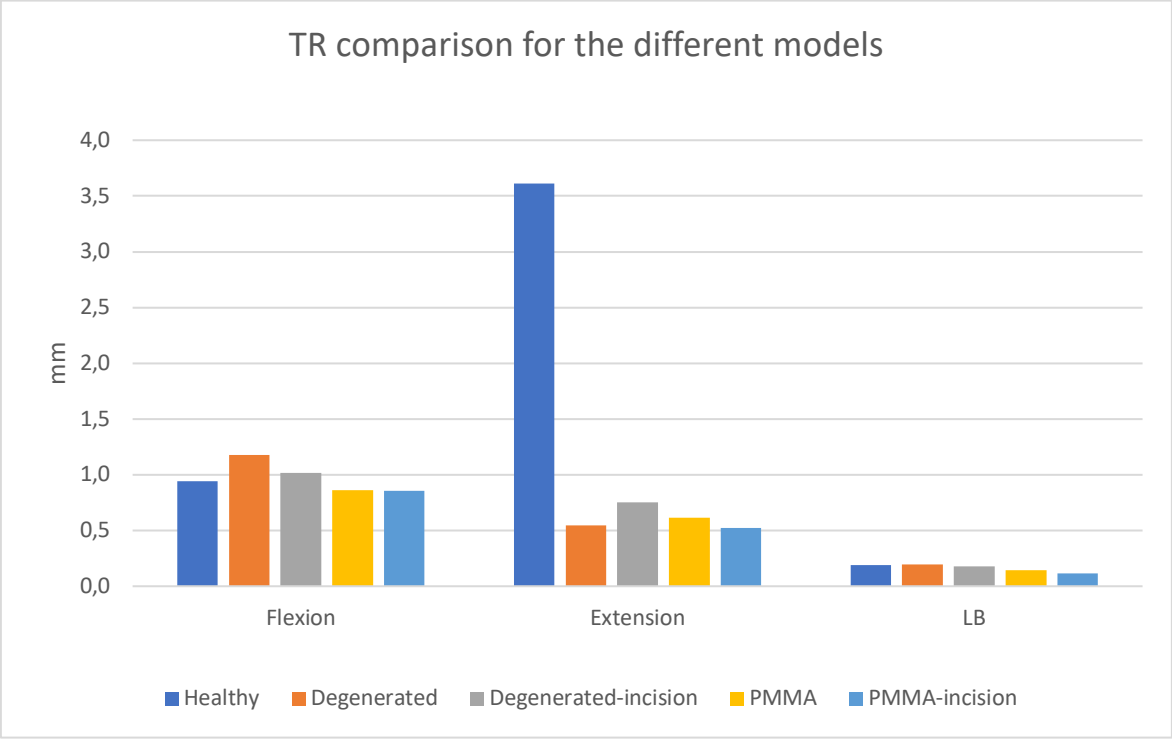

Figure 37. TR comparison among the models depending on the motion.

Following the results observed, Figure 38 shows the calculated normalized TR for degenerated models. In this case, the values are really close to the 100% of the TR of the healthy model (also for the experimental data), except for the extension motion. There is a drastically decrease due to the high value obtained for extension in the simulation of the motions for the healthy model.

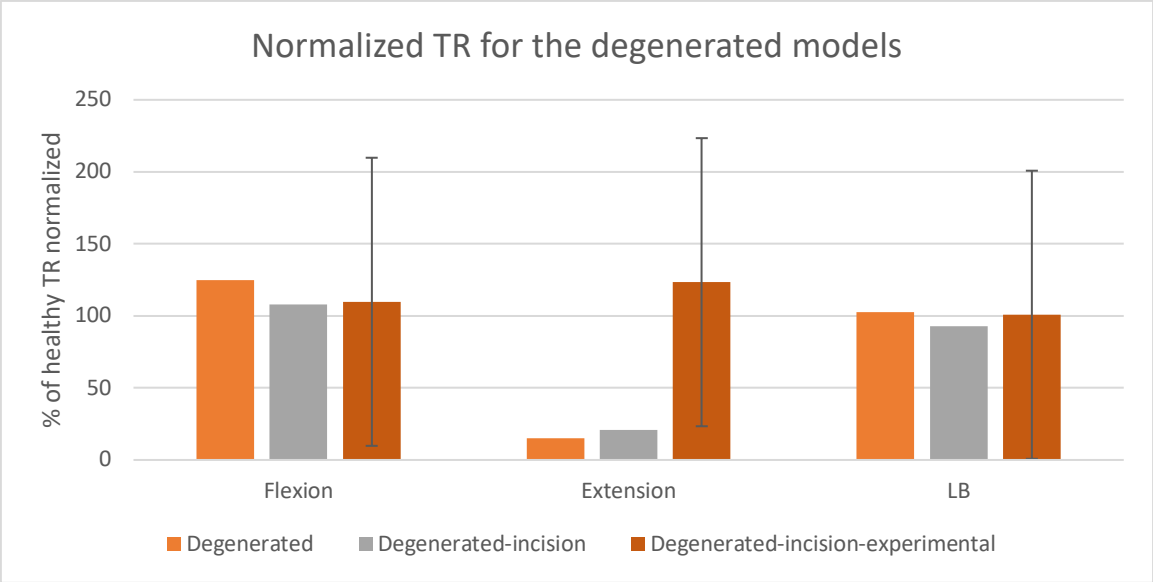

Figure 38. Normalized TRs for the degenerated model compared to the healthy model.

As for normalized TR of the PMMA models (Fig. 39), it is also observable a high decrease of motion for extension as commented before. However, while PMMA and PMMA-incision values seem to have non-statistical differences, the values do not agree with experimental data, that showed an increase of TR when the specimen was cemented.

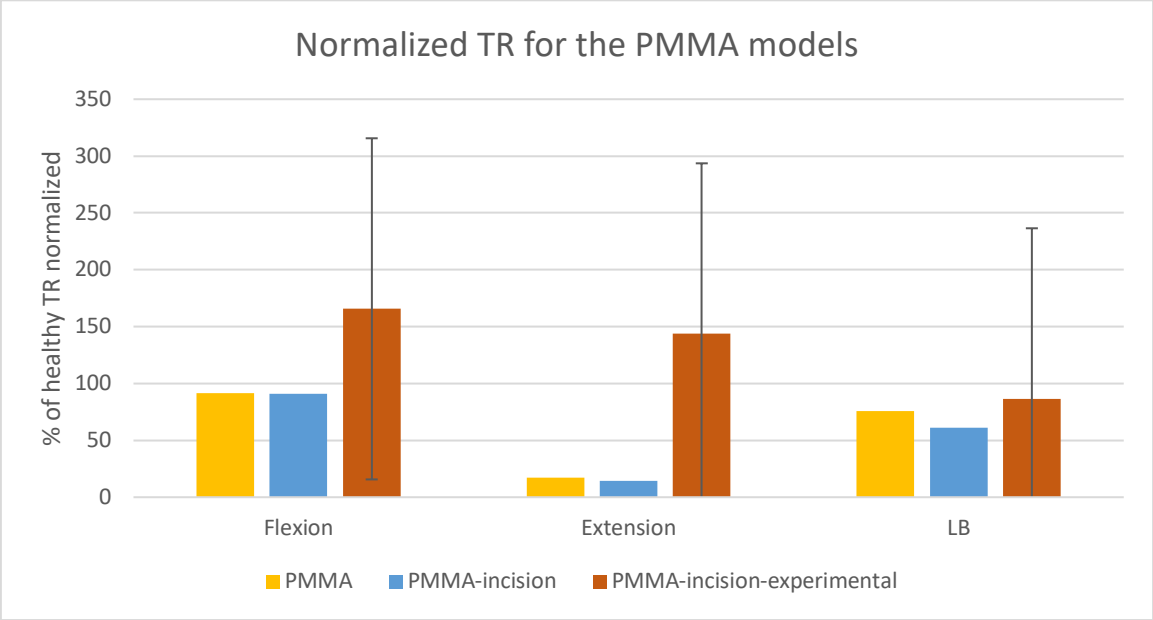

Figure 39. Normalized TRs for the PMMA models compared to healthy motion.

3.3. Strains

As for the intervertebral axial and transversal strains, Figures 40 and 41 respectively show a strain range decrease in both strains for extension compared to flexion, and for lateral bending compared to extension, agreeing with the previous results where ROM values decreased progressively between flexion, extension and lateral bending respectively and also explaining less compression and tension in the intervertebral disc when the lower vertebra has less motion.

As for the degenerated and the degenerated-incision models, statistical differences for every motion and strain values were observed except for axial strain in lateral bending, where the range is similar.

As for the PMMA and PMMA-incision models, both models provided with more or less the same μstrains for every motion and strain values, but in extension and lateral bending the PMMA-incision showed a slightly decreased transversal strain range. As expected, it is shown a decrease in strain range compared to healthy, degenerated and degenerated-incision models.

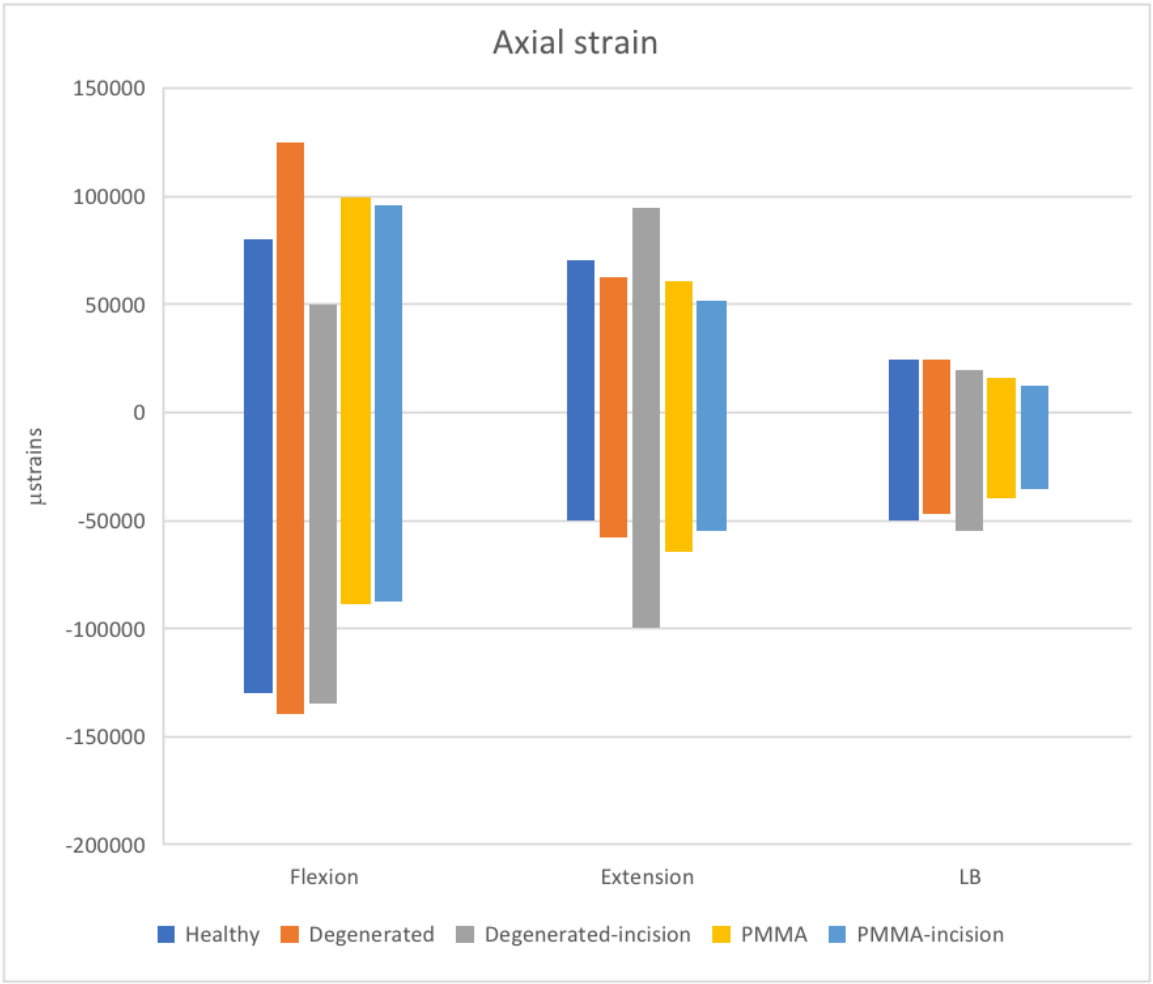

Figure 40. Axial strain of every model depending on the motion.

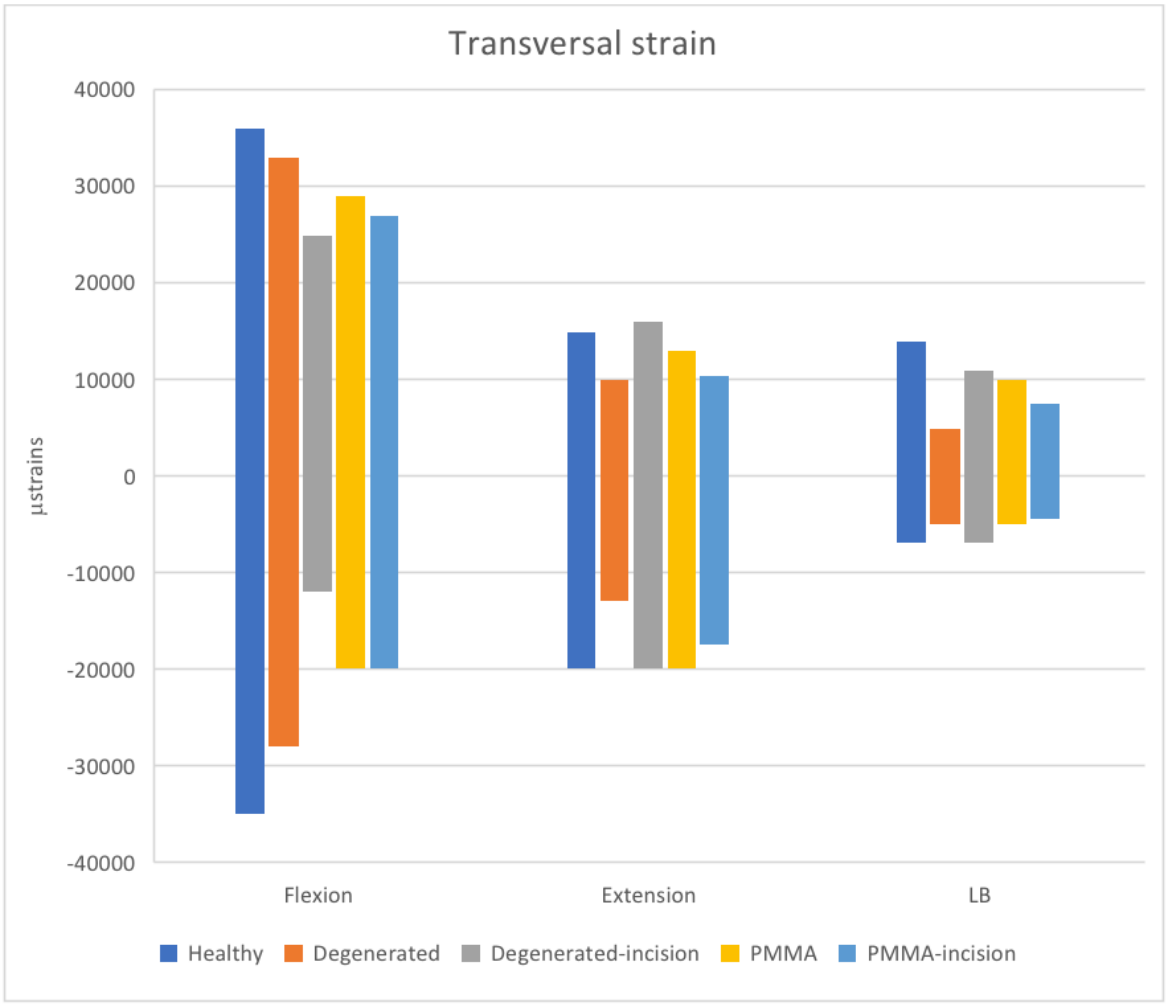

Figure 41. Transversal strain of every model depending on the motion.

4. DISCUSSION

As it was said previously, the aim of the study was to compare the results obtained depending on the intervertebral disc condition (healthy, degenerated, degenerated with an incision, PMMA cemented and PMMA cemented with an incision) depending on the motion (flexion, extension and lateral bending), and also to answer a question that was presented in the Final Degree Thesis: what the effect of the incision inside the annulus is.

Before inquiring into the discussion of the results that were obtained, it must be considered that some of the conditions of the test as the load applied, the model simplifications and the material properties were modified regarding the experimental tests because of the assumptions and the software limitation. This kind of tests submit higher torques and forces to the vertebrae in order to study the behaviour of the spine in the most several cases and, in the current study, lower forces were applied in order to obtain a convergence in the results of the FEM simulations.

Considering these assumptions, the discussion and interpretation of the results obtained are set out below by data output.

4.1. Relative rotation

Firstly, in Figure 32 shows higher rotation for flexion than for extension, and for extension than for lateral bending. This could be explained because of a higher torque generated in flexion as the application of the force is in the upper part of the lower vertebra, whereas in extension and lateral bending the force is applied in the lower part. The force application in flexion was not applied in the lower part of the vertebra due to the lack of distance with the axis of rotation of the lower vertebra, which made a more compressive than rotational motion and implied that the intervertebral disc was compressed without obtaining a rotation.

Figure 33 shows that the values of the ROM for the for the PMMA and PMMA-incision models are lower than for the degenerated and degenerated-incision models. This implies that cemented models are the most rigid than degenerated models. In fact, this is the aim of cementing the vertebra. In addition, it is important to notice that the degenerated models provide with ROMs higher the healthy models as it was expected, since for the degenerated vertebras, the rotations are not damped by the intervertebral disc.

Figure 34 shows that the normalized ROM values for degenerated models seem to be similar between both of them and the experimental data, except for lateral bending, where the degenerated model presented a high increase of ROM compared with the degenerated-incision model and the experimental data.

The normalized ROMs values for the PMMA and PMMA-incision models (Fig. 35) had similar values among them and decreased for every motion, especially for lateral bending motions. The comparison among both, PMMA models and degenerated models also provides with lower values of the normalized ROMs for the PMMA models. This agree with the fact that the PMMA models are more rigid.

4.2. Relative translation

As for the relative translation of the healthy model (Fig. 36 and 37), it is observable a high difference in extension where the lower vertebra drastically moved in the simulation, and this could be a possible outlier that avoids any interpretation of the extension data. However, the normalized graphs (Figs. 38 and 39) showed that cemented models provided lower values of the normalized TRs than the degenerated models, in accordance was it was stated before.

4.3. Strains

For the strain distribution on the intervertebral disc surface, it was obtained the maximum and minimum values of the axial and transversal strain on the surface, being negligible inside the annulus fibrosus and in the nucleus pulposus. As it was explained previously in the Final Degree Thesis, the intervertebral disc has a risk of failure when a load is applied. Degenerated discs entail higher strain values that could lead to tearing the disc, and cementation recovers that risky values [14]. This happens for the axial strains (Figure 40), and only in flexion for the transversal strains (Figure 41). This implies that more accurate models should be developed to study this hypothesis.

As it was discussed previously, maximum and minimum values for both strains are higher in flexion because of the higher ROM obtained, being the intervertebral disc subjected to more tensile and compressive displacements of the tissue in flexion motions. However, this strain data allows to study the differences among the healthy, degenerated and cemented models, but also allows to check the differences of incision and the non-incision models.

As for the differences between incision models, PMMA and PMMA-incision models have non-significant differences, but it is observable a slightly decrease of transversal strain range in extension and lateral bending for the PMMA-incision model. On the other hand, degenerated and degenerated-incision models had significant differences in flexion and extension strain values, but similar results for axial strain in lateral bending.

Thus, strain and ROM results showed some dissimilarities between the incision and non-incision models that probe the possible effect of the incision in the annulus fibrosus.

Ultimately, coinciding with the results obtained in the PCD by Varga et al. and Sola et al., PMMA and PMMA-incision models have a strain distribution decrease due to the distribution of the load in the endplates instead of in the intervertebral disc [25], [26], and this prevents the risk of failure.

4.4. Limitations of the study

In spite of solving some of the problems that appeared in the previous study as the environmental illumination and calibration for the DIC cameras, the use of living beings, the dispersion of the data (the values had huge standard deviations), the strain distribution methodology and the removal of the nucleus pulposus, there are some limitations in this study that difficult the interpretation of the data.

As it was commented before, FEM models need to be simplified because of limitations of the software that is in use or because of the biomechanical behaviour or complexity of the geometry of the vertebrae. Then, the results obtained are compared with the experimental data from the previous study, but the predictivity ability of FEM simulation is just defined for this specific model and conditions [20].

Among the simplifications carried out in the study, it must be considered that the biomechanical behaviour of the annulus fibrosus and the nucleus pulposus is non-linear and viscoelastic and this has not been modelled. Just as the cortical bone has not been distinguished from the trabecular bone. The influence of these behaviours on the results should be analysed.

As for the segmentation methodology that was applied, the generation of the model mesh and segmentation of each part of the vertebrae (upper bone, lower bone and intervertebral disc parts) was poorly performed using a tool from MATLAB that selected each component by calibrating boxes manually. This methodology has been selected due to its easiness and fast performance to segment the different parts of the vertebrae. However, this could be an unsuitable procedure because of the irregularities of some shapes as the intervertebral disc (Fig. 15).

Following with the methodology, the force that generated the rotation of the lower vertebra was applied directly to the lower bone whereas in the previous study the force was applied in a PMMA pot, generating a different momentum between both motions. This pot was not included in any model because of the nodal limitation that has the software ANSYS APDL Academic for the simulation as it was commented previously, and this pot required a high number of elements for its meshing that could compromise the geometry and shape of the vertebrae model.

Last but not least, the results obtained in the simulation are matchless that the ones that were obtained in the experimental data because of the differences in the loading test conditions and recording of data. Only trends have been compared among both methods. An example about the incompatibility of data is that in the DIC method it was manually selected the ROI by selecting the area in the surface as shown in the Figure 6, and this could accidentally select the strain distribution of the endplates. In this study, the segmentation of the intervertebral disc allows obtaining the data without considering the strain distribution in the bone (Fig. 31), being the method of the current study more accurate for data interpretation.

5. CONCLUSION

In conclusion, some of the procedures that were carried out in the current study were advanced compared to the previous one, but others could need an improvement in order to achieve a reliable geometry, material properties and application of forces.

In spite of that, these results allowed to know the similarities between the incision, non-incision and experimental specimen models, where the degenerated-incision model showed very close results to the experimental degenerated model and some dissimilarities with the degenerated model without the incision and the PMMA and PMMA-incision values also showed slightly differences but PMMA-incision had less ROM and strain results, demonstrating that the incision interferes the results between both of them.

Finally, in this simulation it has been proved that for PMMA and PMMA-incision models the ROM decreases compared with healthy models. This result points to a motion reduction of the spine when is applied the PCD due to its stiffness increase and maximum and minimum strain reduction, and this entails less risk of intervertebral disc failure preventing the LBP.

6. REFERENCES

[1] J. A. Waxenbaum and B. Futterman, "Anatomy, Back, Lumbar Vertebrae," in *StatPearls*, Treasure Island (FL): StatPearls Publishing, 2019.

[2] D. Hoy *et al.*, "A systematic review of the global prevalence of low back pain," *Arthritis Rheum.*, vol. 64, no. 6, pp. 2028–2037, 2012, doi: 10.1002/art.34347.

[3] M. A. Adams, "Biomechanics of Back Pain," *Acupunct. Med.*, vol. 22, no. 4, pp. 178–188, Dec. 2002, doi: 10.1136/aim.22.4.178.

[4] M. A. Adams and P. Dolan, "Spine biomechanics," *J. Biomech.*, vol. 38, no. 10, pp. 1972–1983, Oct. 2005, doi: 10.1016/j.jbiomech.2005.03.028.

[5] J. A. Buckwalter, "Aging and Degeneration of the Human Intervertebral Disc," *Spine*, vol. 20, no. 11, p. 1307, Jun. 1995.

[6] H. J. Christie, S. Kumar, and S. A. Warren, "Postural aberrations in low back pain," *Arch. Phys. Med. Rehabil.*, vol. 76, no. 3, pp. 218–224, Mar. 1995, doi: 10.1016/S0003-9993(95)80604-0.

[7] P. N. Sambrook, A. J. MacGregor, and T. D. Spector, "Genetic influences on cervical and lumbar disc degeneration: A magnetic resonance imaging study in twins," *Arthritis Rheum.*, vol. 42, no. 2, pp. 366–372, 1999, doi: 10.1002/1529-0131(199902)42:2<366::AID-ANR20>3.0.CO;2-6.

[8] P.-P. A. Vergroesen *et al.*, "Mechanics and biology in intervertebral disc degeneration: a vicious circle," *Osteoarthritis Cartilage*, vol. 23, no. 7, pp. 1057–1070, Jul. 2015, doi: 10.1016/j.joca.2015.03.028.

[9] J. C. Iatridis, S. B. Nicoll, A. J. Michalek, B. A. Walter, and M. S. Gupta, "Role of biomechanics in intervertebral disc degeneration and regenerative therapies: what needs repairing in the disc and what are promising biomaterials for its repair?," *Spine J.*, vol. 13, no. 3, pp. 243–262, Mar. 2013, doi: 10.1016/j.spinee.2012.12.002.

[10] N. Inoue and A. A. Espinoza Orías, "Biomechanics of Intervertebral Disk Degeneration," *Orthop. Clin. North Am.*, vol. 42, no. 4, pp. 487–499, Oct. 2011, doi: 10.1016/j.ocl.2011.07.001.

[11] R. Gunzburg *et al.*, "A cadaveric study comparing discography, magnetic resonance imaging, histology, and mechanical behavior of the human lumbar disc," *Spine*, vol. 17, no. 4, pp. 417–426, Apr. 1992.

[12] M. Adams, D. McMillan, T. Green, and P. Dolan, "Sustained Loading Generates Stress Concentrations in Lumbar Intervertebral Discs," *Spine*, vol. 21, no. 4, pp. 434–438, Feb. 1996.

[13] P. Pollintine, P. Dolan, J. Tobias, and M. Adams, "Intervertebral Disc Degeneration Can Lead to 'Stress-Shielding' of the Anterior Vertebral Body," *Spine*, vol. 29, no. 7, pp. 774–782, Apr. 2004, doi: 10.1097/01.BRS.0000119401.23006.D2.

[14] G. Collado Soria, "Análisis del comportamiento biomecánico de un disco intervertebral sano, uno degenerado y uno cementado por PMMA," Jun. 08, 2020. https://riunet.upv.es/handle/10251/145701.

[15] A. Nachemson, "The Effect of Forward Leaning on Lumbar Intradiscal Pressure," *Acta Orthop. Scand.*, vol. 35, no. 1–4, pp. 314–328, Jan. 1965, doi: 10.3109/17453676508989362.

[16] H. Wilke, P. Neef, M. Caimi, T. Hoogland, and L. E. Claes, "New In Vivo Measurements of Pressures in the Intervertebral Disc in Daily Life," *Spine*, vol. 24, pp. 755–62, May 1999, doi: 10.1097/00007632-199904150-00005.

[17] M. Al-Rawahi, J. Luo, P. Pollintine, P. Dolan, and M. A. Adams, "Mechanical Function of Vertebral Body Osteophytes, as Revealed by Experiments on Cadaveric Spines:," *Spine*, vol. 36, no. 10, pp. 770–777, May 2011, doi: 10.1097/BRS.0b013e3181df1a70.

[18] B. W. Cunningham, Y. Kotani, P. S. McNulty, A. Cappuccino, and P. C. McAfee, "The effect of spinal destabilization and instrumentation on lumbar intradiscal pressure: an in vitro biomechanical analysis," *Spine*, vol. 22, no. 22, pp. 2655–2663, Nov. 1997.

[19] M. Palanca, G. Tozzi, and L. Cristofolini, "The use of digital image correlation in the biomechanical area: a review," *Int. Biomech.*, vol. 3, no. 1, pp. 1–21, Jan. 2016, doi: 10.1080/23335432.2015.1117395.

[20] M. A. Adams, "Mechanical testing of the spine. An appraisal of methodology, results, and conclusions," *Spine*, vol. 20, no. 19, pp. 2151–2156, Oct. 1995.

[21] R. D. Guyer and D. D. D. M. Ohnmeiss, "Intervertebral Disc Prostheses," *Spine*, vol. 28, no. 15S, pp. 15–23, Aug. 2003.

[22] M. de Kleuver, F. Oner, and W. Jacobs, "Total disc replacement for chronic low back pain: background and a systematic review of the literature," *Eur. Spine J.*, vol. 12, no. 2, pp. 108–116, Apr. 2003, doi: 10.1007/s00586-002-0500-0.

[23] R. Kandel, S. Roberts, and J. P. G. Urban, "Tissue engineering and the intervertebral disc: the challenges," *Eur. Spine J.*, vol. 17, no. Suppl 4, pp. 480–491, Dec. 2008, doi: 10.1007/s00586-008-0746-2.

[24] R. Zhao, W. Liu, T. Xia, and L. Yang, "Disordered Mechanical Stress and Tissue Engineering Therapies in Intervertebral Disc Degeneration," *Polymers*, vol. 11, no. 7, p. 1151, Jul. 2019, doi: 10.3390/polym11071151.

[25] P. P. Varga, G. Jakab, I. B. Bors, A. Lazary, and Z. Szövérfi, "Experiences with PMMA cement as a stand-alone intervertebral spacer," *Orthop.*, vol. 44, no. 1, pp. 1–8, Nov. 2015, doi: 10.1007/s00132-014-3060-1.

[26] C. Sola *et al.*, "Percutaneous cement discoplasty for the treatment of advanced degenerative disk disease in elderly patients," *Eur. Spine J. Off. Publ. Eur. Spine Soc. Eur. Spinal Deform. Soc. Eur. Sect. Cerv. Spine Res. Soc.*, Mar. 2018, doi: 10.1007/s00586-018-5547-7.

[27] M. Palanca, T. M. Brugo, and L. Cristofolini, "Use of digital image correlation to investigate the biomechanics of the vertebra," *J. Mech. Med. Biol.*, vol. 15, no. 02, p. 1540004, Apr. 2015, doi: 10.1142/S0219519415400047.

[28] T. J. Keating, P. R. Wolf, and F. L. Scarpace, "An improved method of digital image correlation," *Am Soc Photogr Rem Sens*, vol. 41, p. 10, Aug. 1975.

[29] B. K. Bay, S. A. Yerby, R. F. McLain, and E. Toh, "Measurement of strain distributions within vertebral body sections by texture correlation," *Spine*, vol. 24, no. 1, pp. 10–17, Jan. 1999.

[30] M. L. Ruspi, M. Palanca, C. Faldini, and L. Cristofolini, "Full-field in vitro investigation of hard and soft tissue strain in the spine by means of Digital Image Correlation," *Muscles Ligaments Tendons J.*, vol. 7, no. 4, pp. 538–545, Apr. 2018, doi: 10.11138/mltj/2017.7.4.538.

[31] M. Palanca *et al.*, "Digital volume correlation can be used to estimate local strains in natural and augmented vertebrae: An organ-level study," *J. Biomech.*, vol. 49, no. 16, pp. 3882–3890, Dec. 2016, doi: 10.1016/j.jbiomech.2016.10.018.

[32] A. Rohlmann, T. Zander, H. Schmidt, H.-J. Wilke, and G. Bergmann, "Analysis of the influence of disc degeneration on the mechanical behaviour of a lumbar motion segment using the finite element method," *J. Biomech.*, vol. 39, no. 13, pp. 2484–2490, Jan. 2006, doi: 10.1016/j.jbiomech.2005.07.026.

[33] G. Denozière and D. N. Ku, "Biomechanical comparison between fusion of two vertebrae and implantation of an artificial intervertebral disc," *J. Biomech.*, vol. 39, no. 4, pp. 766–775, Jan. 2006, doi: 10.1016/j.jbiomech.2004.07.039.

[34] S. M. Renner *et al.*, "Novel model to analyze the effect of a large compressive follower pre-load on range of motions in a lumbar spine," *J. Biomech.*, vol. 40, no. 6, pp. 1326–1332, 2007, doi: 10.1016/j.jbiomech.2006.05.019.

[35] J. P. Little, C. J. Adam, J. H. Evans, G. J. Pettet, and M. J. Pearcy, "Nonlinear finite element analysis of anular lesions in the L4/5 intervertebral disc," *J. Biomech.*, vol. 40, no. 12, pp. 2744–2751, Jan. 2007, doi: 10.1016/j.jbiomech.2007.01.007.

[36] L. M. Ruberté, R. N. Natarajan, and G. BJ. Andersson, "Influence of single-level lumbar degenerative disc disease on the behavior of the adjacent segments—A finite element model study," *J. Biomech.*, vol. 42, no. 3, pp. 341–348, Feb. 2009, doi: 10.1016/j.jbiomech.2008.11.024.

[37] S. A. Shirazi-Adl, S. C. Shrivastava, and A. M. Ahmed, "Stress Analysis of the Lumbar Disc-Body Unit in Compression A Three-Dimensional Nonlinear Finite Element Study," *Spine*, vol. 9, no. 2, pp. 120–134, Mar. 1984.

[38] V. K. Goel, W. Kong, J. S. Han, J. N. Weinstein, and L. G. Gilbertson, "A Combined Finite Element and Optimization Investigation of Lumbar Spine Mechanics With and Without Muscles," *Spine*, vol. 18, no. 11, pp. 1531–1541, Sep. 1993.

[39] N. Newell, J. Little, A. Christou, M. Adams, C. Adam, and S. Masouros, "Biomechanics of the human intervertebral disc: A review of testing techniques and results," *J. Mech. Behav. Biomed. Mater.*, vol. 69, pp. 420–434, May 2017, doi: 10.1016/j.jmbbm.2017.01.037.

[40] M. M. Bouziane, H. Salah, S. Benbarek, B. A. Bouiadjra, and B. Serier, "Finite Element Analysis of the Mechanical Behaviour of a Reinforced PMMA-Based Hip Spacer," *Adv. Mater. Res.*, vol. 1105, pp. 36–40, May 2015, doi: 10.4028/www.scientific.net/AMR.1105.36.

BUDGET

7. Budget

7.1. Introduction

The Final Master's Degree Thesis was performed in his totality by telecommunication without requiring any biomechanical installation or living beings to its study. However, it was necessary some specific tools and activities that need to sum up the budget by chapters.

It has been considered the number of hours necessary to the Master's Thesis (20 credits) dedicated for every activity, the licensing, machinery and materials that were used during the study.

The contents of this present budget document are:

- Labour costs: prices of the work done by the staff of the study.
- Material costs: software licensing and material purchases.
- Machinery costs: tools required for the simulations.
- Sub-budgets: budgets ordered by activity.
- Budgets by unit: definition of the activity costs in numerals and letters.
- Price breakdown: activity prices considering their needs and direct and indirect costs.
- Total budget: overall spent in the study.

7.2. Labour costs

Nº	Code	Description	Qty	Price	Total
1	LC.BE	Biomedical engineer	500 h	15,00€/h	7.500€
				Sub Total	**7.500€**

7.3. Material costs

Nº	Code	Description	Qty	Payback factor	Price	Total
1	MAT.MTL	MATLAB R2020a license	1 u	5/12	800,00€/u	333,33€
2	MAT.ANS	ANSYS Student 2020 R2 license	1 u	5/12	0€/u	0€
3	MAT.OFF	Microsoft Office 365 (2018) license	1 u	5/12	69,00€/u	28,75€
4	MAT.3DS	3DSlicer license	1 u	5/12	0€/u	0€
5	MAT.PRN	Thesis printing	42 u	-	0,10€/u	4,20€
6	MAT.BIN	Bookbinding	1 u	-	10,00€/u	10 €
					Sub Total	**376,28€**

7.4. Machinery costs

Nº	Code	Description	Qty	Payback factor	Price	Total
1	MAC.PC	Custom PC with Windows 10 Pro	1 u	5/12	1.000,00€/u	416,67€
2	MAC.MBK	MacBook Pro Retina 13’ 2015	1 u	5/12	1.400,00€/u	583,33€
					Sub Total	**1.000,00€**

7.5. Sub-budgets

- **Sub-budget nº1: Literature and Thesis planning**

Nº	Unit	Description	Qty	Price	Total
1.1	h	Literature and research	40	15,45€/h	618,00€
1.2.	h	Tutor meetings	10	15,45€/h	154,50€
				Sub Total	**772,50€**

- **Sub-budget nº2: Hardware, software and programming**

Nº	Unit	Description	Qty	Price	Total
2.1	u	Hardware and software installation	1	1.402,94€/u	1.402,94€
2.2	h	MATLAB codes	200	15,45€/h	3.090,00€
				Sub Total	**4.492,94€**

- **Sub-budget nº3: Modelling and simulations**

Nº	Unit	Description	Qty	Price	Total
3.1	h	Model segmentation	20	15,45€/h	309,00€
3.2	h	Model meshing	20	15,45€/h	309,00€
3.3	h	ANSYS APDL simulations	20	15,45€/h	309,00€
				Sub Total	**927,00€**

- **Sub-budget nº4: Document drafting, printing and Thesis defense**

Nº	Unit	Description	Qty	Price	Total
4.1	h	Thesis, budget and appendix	160	15,45€/h	2.472,00€
4.2	h	Thesis defense	30	15,45€/h	463,50€
4.3	u	Thesis printing	1	14,62€/u	14,62€
				Sub Total	**2.950,12€**

7.6. Budgets by units

Nº	Description	Costs (€)	
		Numeral	Letter
	Sub-budget nº1: Literature and Thesis planning		
1.1	Literature and research (h)	15,45	Fifteen euros and forty-five cents
1.2	Tutor meetings (h)	15,45	Fifteen euros and forty-five cents
	Sub-budget nº2: Hardware, software and programming		
2.1	Hardware and software installation (u)	1.402,94	One thousand four hundred and two euros and ninety-four cents
2.2	MATLAB codes (h)	15,45	Fifteen euros and forty-five cents
	Sub-budget nº3: Modelling and simulations		
3.1	Model segmentation (h)	15,45	Fifteen euros and forty-five cents
3.2	Model meshing (h)	15,45	Fifteen euros and forty-five cents
3.3	ANSYS APDL simulations (h)	15,45	Fifteen euros and forty-five cents
	Sub-budget nº4: Document drafting, printing and Thesis defense		
4.1	Thesis, budget and appendix (h)	15,45	Fifteen euros and forty-five cents
4.2	Thesis defense (h)	15,45	Fifteen euros and forty-five cents
4.3	Thesis printing (u)	14,62	Fifteen euros and sixty-two cents

7.7. Price breakdown

Nº	U	Description				Total
		Sub-budget nº1: Literature and Thesis planning				
1.1	h	Literature and research				
		LC.BE	1 h	Biomedical engineer	15,00€/h	15,00€
		%001	1 %	Direct costs	15,00€	0,15€
		%002	2 %	Indirect costs	15,00€	0,30€
					Price/h	**15,45€**
1.2	h	Tutor meetings				
		LC.BE	1 h	Biomedical engineer	15,00€/h	15,00€
		%001	1 %	Direct costs	15,00€	0,15€
		%002	2 %	Indirect costs	15,00€	0,30€
					Price/h	**15,45€**
		Sub-budget nº2: Hardware, software and programming				
2.1	h	Hardware and software installation				
		MAC.PC	1 u	Custom PC with Windows 10 Pro	(5/12) 1000€/u	416,67€
		MAC.MBK	1 u	MacBook Pro Retina 13’ 2015	(5/12) 1400€/u	583,33€
		MAT.3DS	1 u	3DSlicer license	(5/12) 0€/u	0 €
		MAT.MTL	1 u	MATLAB R2020a license	(5/12) 800€/u	333,33€
		MAT.ANS	1 u	ANSYS Student 2020 R2 license	(5/12) 0€/u	0€
		MAT.OFF	1 u	Microsoft Office 365 (2018) license	(5/12) 69€/u	28,75€
		%001	1 %	Direct costs	1362,08€	13,62€
		%002	2 %	Indirect costs	1362,08€	27,24€
					Price/h	**1.402,94€**
2.2	h	MATLAB codes				
		LC.BE	1 h	Biomedical engineer	15,00€/h	15,00€
		%001	1 %	Direct costs	15,00€	0,15€
		%002	2 %	Indirect costs	15,00€	0,30€
					Price/h	**15,45€**

Nº	U	Description				Total
		Sub-budget nº3: Modelling and simulations				
3.1	h	Model segmentation				
		LC.BE	1 h	Biomedical engineer	15,00€/h	15,00€
		%001	1 %	Direct costs	15,00€	0,15€
		%002	2 %	Indirect costs	15,00€	0,30€
					Price/h	**15,45€**
3.2	h	Model meshing				
		LC.BE	1 h	Biomedical engineer	15,00€/h	15,00€
		%001	1 %	Direct costs	15,00€	0,15€
		%002	2 %	Indirect costs	15,00€	0,30€
					Price/h	**15,45€**
3.3	h	ANSYS APDL simulations				
		LC.BE	1 h	Biomedical engineer	15,00€/h	15,00€
			1 %	Direct costs	15,00€	0,15€
			2 %	Indirect costs	15,00€	0,30€
					Price/h	**15,45€**
		Sub-budget nº4: Document drafting, printing and Thesis defense				
4.1	h	Thesis, budget and appendix				
		LC.BE	1 h	Biomedical engineer	15,00€/h	15,00€
		%001	1 %	Direct costs	15,00€	0,15€
		%002	2 %	Indirect costs	15,00€	0,30€
					Price/h	**15,45€**
4.2	h	Thesis defense				
		LC.BE	1 h	Biomedical engineer	15,00€/h	15,00€
		%001	1 %	Direct costs	15,00€	0,15€
		%002	2 %	Indirect costs	15,00€	0,30€
					Price/h	**15,45€**
4.3	u	Thesis printing				
		MAT.PRN	1 u	Thesis printing	4,20€/u	4,20€
		MAT.BIN	1 u	Bookbinding	10,00€/u	10,00€
		%001	1 %	Direct costs	14,20€	0,14€
		%002	2 %	Indirect costs	14,20€	0,28€
					Price/u	**14,62€**

7.8. Total budget

Sub-budget	Total
Sub-budget nº1: Literature and Thesis planning	772,50€
Sub-budget nº2: Hardware, software and programming	4.492,94€
Sub-budget nº3: Modelling and simulations	927,00€
Sub-budget nº4: Document drafting, printing and Thesis defense	2.950,12€
Sub Total	9.142,56€
General expenditure (13%)	1.188,53€
Industrial benefits (6%)	548,55€
Execution budget per contract	10.879,64€
VAT (21%)	2.284,72€
Overall tender budget	**13.164,36€**

The overall tender budget amounts to a **thirteen thousand one hundred and sixty-four euros and thirty-six cents.**

APPENDIX

APPENDIX I: Code for meshing and material assignments from a .stl to a .ans file

```
%% Author: Guillermo Collado Soria
% Mesh generator from a Healthy.stl file created in 3DSlicer

clear
clc
close all

%% Mesh creation
for i=1:6 % Loop for creating different mesh sizes from 1 to
6

clearvars -except i % Restart variables for the next loop

tic % Start cronometer

figure
model = createpde(1);
importGeometry(model,'Healthy.stl'); % .stl model import

% Mesh generation
Mesh =
generateMesh(model,'Hmax',i,'Hmin',i,'GeometricOrder','linea
r') % Tetrahedral mesh with an element size from 1 to 6
nodes = model.Mesh.Nodes'; % List of every node of the mesh
elements = model.Mesh.Elements'; % List of every element of
the mesh


%% Detection of the elements of each part of the model by
manual selection
% Nucleus pulposus elements
nucleus_elements = findElements(mesh,'box',[-38 -17],[102
115],[678 686]); % Box that contains inside the nucleus
pulposus elements

% Anulus fibrosus elements
disc_elements1 = findElements(mesh,'box',[-999 999],[95
999],[678.5 686]); % Box that contains inside the
intervertebral disc elements (included the nucleus pulposus
elements)
n1=1;
% Loop for eliminating the nucleus pulposus elements from
the intervertebral disc box
for k =1:length(disc_elements1)
if disc_elements1(k) ~= nucleus_elements % Detection of the
nucleus pulposus elements to avoid them
   disc_elements(n1) = disc_elements1(k); % Variable with
only the annulus fibrosus elements
```

```
    n1=n1+1;
end
end


% Upper vertebra elements
upper_elements1 = findElements(mesh,'box',[-999 999],[-999
999 ],[682 999]); % Box that contains inside the upper bone
elements (included some intervertebral disc elements)
k1=1;
% Loop for eliminating the intervertebral disc elements from
the upper bone box
for k =1:length(upper_elements1)
if upper_elements1(k) ~= disc_elements % Avoid annulus
fibrosus elements
    if upper_elements1(k) ~= nucleus_elements % Avoid nucleus
pulposus elements
    upper_elements(k1) = upper_elements1(k); % Variable with
only the upper bone elements
    k1=k1+1;
end
end
end

% Lower vertebra elements
lower_elements1 = findElements(mesh,'box',[-999 999],[-999
999 ],[0 684]); % Box that contains inside the lower bone
elements (included some intervertebral disc elements)
k2=1;
% Loop for eliminating the intervertebral disc elements from
the lower bone box
for h =1:length(lower_elements1)
if lower_elements1(h) ~= disc_elements % Avoid annulus
fibrosus elements
    if lower_elements1(h) ~= nucleus_elements % Avoid nucleus
pulposus elements
    lower_elements(k2) = lower_elements1(h); % Variable with
only the lower bone elements
    k2=k2+1;
end
end
end

% Representation of the model
subplot (1,2,1) % Model
pdemesh(mesh.Nodes,mesh.Elements(:,upper_elements),'FaceColo
r','green')
hold on
pdemesh(mesh.Nodes,mesh.Elements(:,disc_elements),'FaceColor
','red')
hold on
```

```
pdemesh(mesh.Nodes,mesh.Elements(:,lower_elements),'FaceColo
r','blue')
hold on
pdemesh(mesh.Nodes,mesh.Elements(:,nucleus_elements),'FaceCo
lor','yellow')

% Representation of the annulus fibrosus and the nucleus
pulposus
subplot (1,2,2)
pdemesh(mesh.Nodes,mesh.Elements(:,disc_elements),'FaceColor
','red')
hold on
pdemesh(mesh.Nodes,mesh.Elements(:,nucleus_elements),'FaceCo
lor','yellow')


%% ANSYS file creation

% Opening of a new .ans file
file = sprintf('HEALTHY_MESH %d', i);
fid = fopen([file '.ans'],'w+');

% Heading
fprintf(['Writing header... ' file '.ans\n']);

fprintf(fid, '/TITLE, Ansys export from Matlab\n');
fprintf(fid, '!----------------------------------------\n');
fprintf(fid, '!Enter general input data preprocessor\n');
fprintf(fid, '/PREP7\n');
fprintf(fid, '!----------------------------------------
--------\n');
fprintf(fid,
'!=====================================================\n');
% Material definitions
fprintf(fid, '!MATERIAL DEFINITIONS BEGIN\n');
fprintf(fid,
'!=====================================================\n');
fprintf(fid, '!MP,[Lab],[MAT],[C0],[C1,C2,C3,C4]\n');
fprintf(fid,
'!=====================================================\n');
% Bone material properties
fprintf(fid, '!MATERIAL PLACEHOLDER BEGIN\n');
fprintf(fid, '!Part: Bone\n');
fprintf(fid, '!Part Material: BONE\n');
fprintf(fid, 'MP,EX,1,1.2e+04,0,0,0,0 \n'); % 12.000 MPa
Young Modulus
fprintf(fid, 'MP,PRXY,1,0.3,0,0,0,0 \n'); % 0.3 Poisson
Ratio
fprintf(fid, '!MATERIAL PLACEHOLDER END\n');
fprintf(fid,
'!=====================================================\n');
```

```
fprintf(fid,
'!=====================================================\n');

% Annulus fibrosus properties
fprintf(fid, '!!MATERIAL PLACEHOLDER BEGIN\n');
fprintf(fid, '!Part: Disc\n');
fprintf(fid, '!Part Material: Disc\n');
fprintf(fid, 'MP,EX,2,655,0,0,0,0 \n'); % 655 MPa Young
Modulus
fprintf(fid, 'MP,PRXY,2,0.3,0,0,0,0 \n'); % 0.3 Poisson
Ratio
fprintf(fid, '!MATERIAL PLACEHOLDER END\n');
fprintf(fid,
'!=====================================================\n');
fprintf(fid,
'!=====================================================\n');

% Nucleus pulposus properties
fprintf(fid, '!!MATERIAL PLACEHOLDER BEGIN\n');
fprintf(fid, '!Part: Nucleuspulposus\n');
fprintf(fid, '!Part Material: NUCLEUSPULPOSUS\n');
fprintf(fid, 'MP,EX,3,1,0,0,0,0 \n'); % 1 MPa Young Modulus
fprintf(fid, 'MP,PRXY,3,0.49,0,0,0,0 \n'); % 0.49 Poisson
Ratio
fprintf(fid, '!MATERIAL PLACEHOLDER END\n');
fprintf(fid,
'!=====================================================\n');
fprintf(fid,
'!=====================================================\n');

% PMMA properties (Not used in healthy model)
fprintf(fid, '!!MATERIAL PLACEHOLDER BEGIN\n');
fprintf(fid, '!Part: PMMA\n');
fprintf(fid, '!Part Material: PMMA\n');
fprintf(fid, 'MP,EX,4,2.7e+03,0,0,0,0 \n'); % 2700 MPa Young
Modulus
fprintf(fid, 'MP,PRXY,4,0.49,0,0,0,0 \n'); % 0.35 Poisson
Ratio
fprintf(fid, '!MATERIAL PLACEHOLDER END\n');
fprintf(fid,
'!=====================================================\n');
fprintf(fid,
'!=====================================================\n');

fprintf(fid, '!MATERIAL DEFINITIONS END\n');
fprintf(fid,
'!=====================================================\n');
fprintf(fid,
'!=====================================================\n');

fprintf(fid, '!CONTACT DEFINITIONS BEGIN\n');
```

```
fprintf(fid,
'!====================================================\n');
fprintf(fid,
'!====================================================\n');
fprintf(fid, '!CONTACT DEFINITIONS END\n');

% Nodes
fprintf(fid,
'!====================================================\n');
fprintf(fid,
'!====================================================\n');
fprintf(fid, '!NODE DATA BEGIN\n');
fprintf(fid,
'!====================================================\n');
fprintf(fid, '!-------------------------------------------
--------\n');
fprintf(fid, '!N,[NODE INDEX],[X COORD],[Y COORD],[Z
COORD]\n');
fprintf(fid, '!-------------------------------------------
--------\n');

for n=1:size(nodes,1)
    fprintf(fid, '%c, %i, %d, %d,
%d\r\n','N',n,nodes(n,1),nodes(n,2),nodes(n,3));
end

fprintf(fid, '!-------------------------------------------
--------\n');
fprintf(fid, 'NSEL, NONE\n');
fprintf(fid, '!-------------------------------------------
--------\n');
fprintf(fid,
'!====================================================\n');
fprintf(fid, '!NODE DATA END\n');

% Elements
fprintf(fid,
'!====================================================\n');
fprintf(fid,
'!====================================================\n');
fprintf(fid, '!SOLID ELEMENT DATA BEGIN\n');
fprintf(fid,
'!====================================================\n');
fprintf(fid, '!-------------------------------------------
--------\n');
fprintf(fid, '!Linear tetrahedral elements\n');
fprintf(fid, 'ET, 1, SOLID185\n');
fprintf(fid, '!-------------------------------------------
--------\n');
fprintf(fid,
'!====================================================\n');
```

```
fprintf(fid, '!ELEMENTS - Part: Upperbone BEGIN\n');
fprintf(fid, '!Part Material: Upperbone\n');
fprintf(fid, '!Material ID: PM_Bone\n');
fprintf(fid, '!Material Index: 1\n');
fprintf(fid, '!-------------------------------------------
--------\n');
fprintf(fid, 'ESEL, NONE\n');
fprintf(fid, '!-------------------------------------------
--------\n');
fprintf(fid,
'!=====================================================\n');

% Upper bone definition
fprintf(fid, '!ELEMENTS (TETRAHEDRA) - Part: Upperbone
BEGIN\n');
fprintf(fid, 'TYPE, 1\n');
fprintf(fid, '!-------------------------------------------
--------\n');
fprintf(fid, 'MAT, 1\n'); % Bone material
fprintf(fid, '!-------------------------------------------
--------\n');
for e1=1:size(upper_elements,2)
    fprintf(fid, '%s, %i, %d, %d, %d,
%d\r\n','EN',e1,elements(upper_elements(e1),1),elements(uppe
r_elements(e1),2),elements(upper_elements(e1),3),elements(up
per_elements(e1),4));
end
fprintf(fid, '**ELEMENTS (TETRAHEDRA) - Part: Upperbone
END\n');
fprintf(fid, '!ELEMENTS (TETRAHEDRA) - Part: Upperbone
END\n');
fprintf(fid,
'!=====================================================\n');
fprintf(fid, '!-------------------------------------------
--------\n');
fprintf(fid, '!CM, Cname, Entity type - Group geometry items
(preceding elements) into a component\n');
fprintf(fid, 'CM, PT_UPPERBONE, ELEM\n');
fprintf(fid, 'ESEL, NONE\n');
fprintf(fid, '!-------------------------------------------
--------\n');
fprintf(fid, '!ELEMENTS - Part: Upperbone END\n');
fprintf(fid,
'!=====================================================\n');
fprintf(fid,
'!=====================================================\n');

% Lower bone definition
fprintf(fid, '!ELEMENTS - Part: Lowerbone BEGIN\n');
fprintf(fid, '!Part Material: Lowerbone\n');
fprintf(fid, '!Material ID: PM_Bone\n');
fprintf(fid, '!Material Index: 1\n');
```

```
fprintf(fid, '!-----------------------------------------
--------\n');
fprintf(fid, 'ESEL, NONE\n');
fprintf(fid, '!-----------------------------------------
--------\n');
fprintf(fid,
'!=====================================================\n');
fprintf(fid, '!ELEMENTS (TETRAHEDRA) - Part: Lowerbone
BEGIN\n');
fprintf(fid, 'TYPE, 1\n');
fprintf(fid, '!-----------------------------------------
--------\n');
fprintf(fid, 'MAT, 1\n'); % Bone material
fprintf(fid, '!-----------------------------------------
--------\n');
for e2=1:size(lower_elements,2)
    fprintf(fid, '%s, %i, %d, %d, %d,
%d\r\n','EN',e2+size(upper_elements,2),elements(lower_elemen
ts(e2),1),elements(lower_elements(e2),2),elements(lower_elem
ents(e2),3),elements(lower_elements(e2),4));
end
fprintf(fid, '**ELEMENTS (TETRAHEDRA) - Part: Lowerbone
END\n');
fprintf(fid, '!ELEMENTS (TETRAHEDRA) - Part: Lowerbone
END\n');
fprintf(fid,
'!=====================================================\n');
fprintf(fid, '!-----------------------------------------
--------\n');
fprintf(fid, '!CM, Cname, Entity type - Group geometry items
(preceding elements) into a component\n');
fprintf(fid, 'CM, PT_LOWERBONE, ELEM\n');
fprintf(fid, 'ESEL, NONE\n');
fprintf(fid, '!-----------------------------------------
--------\n');
fprintf(fid, '!ELEMENTS - Part: Lowerbone END\n');
fprintf(fid,
'!=====================================================\n');
fprintf(fid,
'!=====================================================\n');

% Annulus fibrosus definition
fprintf(fid, '!ELEMENTS - Part: Disc BEGIN\n');
fprintf(fid, '!Part Material: Disc\n');
fprintf(fid, '!Material ID: PM_Disc\n');
fprintf(fid, '!Material Index: 2\n');
fprintf(fid, '!-----------------------------------------
--------\n');
fprintf(fid, 'ESEL, NONE\n');
fprintf(fid, '!-----------------------------------------
--------\n');
```

```
fprintf(fid,
'!=====================================================\n');
fprintf(fid, '!ELEMENTS (TETRAHEDRA) - Part: Disc BEGIN\n');
fprintf(fid, 'TYPE, 1\n');
fprintf(fid, '!-----------------------------------------
--------\n');
fprintf(fid, 'MAT, 2\n'); % Annulus fibrosus material
fprintf(fid, '!-----------------------------------------
--------\n');
for e3=1:size(disc_elements,2)
    fprintf(fid, '%s, %i, %d, %d, %d,
%d\r\n','EN',e3+size(upper_elements,2)+size(lower_elements,2
),elements(disc_elements(e3),1),elements(disc_elements(e3),2
),elements(disc_elements(e3),3),elements(disc_elements(e3),4
));
end
fprintf(fid, '**ELEMENTS (TETRAHEDRA) - Part: Disc END\n');
fprintf(fid, '!ELEMENTS (TETRAHEDRA) - Part: Disc END\n');
fprintf(fid,
'!=====================================================\n');
fprintf(fid, '!-----------------------------------------
--------\n');
fprintf(fid, '!CM, Cname, Entity type - Group geometry items
(preceding elements) into a component\n');
fprintf(fid, 'CM, PT_DISC, ELEM\n');
fprintf(fid, 'ESEL, NONE\n');
fprintf(fid, '!-----------------------------------------
--------\n');
fprintf(fid, '!ELEMENTS - Part: DISC END\n');
fprintf(fid,
'!=====================================================\n');
fprintf(fid,
'!=====================================================\n');

% Nucleus pulposus definition
fprintf(fid, '!ELEMENTS - Part: Nucleuspulposus BEGIN\n');
fprintf(fid, '!Part Material: Nucleuspulposus\n');
fprintf(fid, '!Material ID: PM_Nucleuspulposus\n');
fprintf(fid, '!Material Index: 3\n');
fprintf(fid, '!-----------------------------------------
--------\n');
fprintf(fid, 'ESEL, NONE\n');
fprintf(fid, '!-----------------------------------------
--------\n');
fprintf(fid,
'!=====================================================\n');
fprintf(fid, '!ELEMENTS (TETRAHEDRA) - Part: Nucleuspulposus
BEGIN\n');
fprintf(fid, 'TYPE, 1\n');
fprintf(fid, '!-----------------------------------------
--------\n');
fprintf(fid, 'MAT, 3\n'); % Nucleus pulposus material
```

```
fprintf(fid, '!-----------------------------------------
--------\n');
for e4=1:size(nucleus_elements,2)
    fprintf(fid, '%s, %i, %d, %d, %d,
%d\r\n','EN',e4+size(upper_elements,2)+size(lower_elements,2
)+size(disc_elements,2),elements(nucleus_elements(e4),1),ele
ments(nucleus_elements(e4),2),elements(nucleus_elements(e4),
3),elements(nucleus_elements(e4),4));
end
fprintf(fid, '**ELEMENTS (TETRAHEDRA) - Part:
Nucleuspulposus END\n');
fprintf(fid, '!ELEMENTS (TETRAHEDRA) - Part: Nucleuspulposus
END\n');
fprintf(fid,
'!=====================================================\n');
fprintf(fid, '!-----------------------------------------
--------\n');
fprintf(fid, '!CM, Cname, Entity type - Group geometry items
(preceding elements) into a component\n');
fprintf(fid, 'CM, PT_NUCLEUSPULPOSUS, ELEM\n');
fprintf(fid, 'ESEL, NONE\n');
fprintf(fid, '!-----------------------------------------
--------\n');
fprintf(fid, '!ELEMENTS - Part: Nucleuspulposus END\n');
fprintf(fid,
'!=====================================================\n');
fprintf(fid,
'!=====================================================\n');

fprintf(fid, '!SOLID ELEMENT DATA END\n');
fprintf(fid,
'!=====================================================\n');
fprintf(fid,
'!=====================================================\n');
fprintf(fid, '!SHELL ELEMENT DATA BEGIN\n');
fprintf(fid,
'!=====================================================\n');
fprintf(fid,
'!=====================================================\n');
fprintf(fid, '!SHELL ELEMENT DATA END\n');
fprintf(fid,
'!=====================================================\n');
fprintf(fid,
'!=====================================================\n');
fprintf(fid, '!CONTACT SURFACE DATA BEGIN\n');
fprintf(fid,
'!=====================================================\n');
fprintf(fid,
'!=====================================================\n');
fprintf(fid, '!CONTACT SURFACE DATA END\n');
fprintf(fid,
'!=====================================================\n');
```

```
fprintf(fid, '!-----------------------------------------
--------\n');
fprintf(fid, '!Select all & exit general input data
preprocessor (/PREP7)\n');
fprintf(fid, 'ALLSEL\n');
fprintf(fid, 'FINISH\n');
fprintf(fid, '!-----------------------------------------
--------\n');

% Saving the generated .ans file
fclose(fid);
fprintf(['Input file ' file '.ans has been created\n']);

toc % End cronometer

end
```

APPENDIX II: Code for the calculation of the angle and translation of the lower vertebra

```
%% Author: Guillermo Collado Soria
% ROM angle and relative translation calculation for healthy
model

clear all
close all
clc

%% Extracting the nodes from the generated .ans file that
contained the initial position of the nodes
load('Healthy_nodes.mat'); % .mat that contains the nodes of
the .ans file with 2.5 element size

x = HEALTHYMESH2(:,2); % X coordinates
y = HEALTHYMESH2(:,3); % Y coordinates
z = HEALTHYMESH2(:,4); % Z coordinates

% Vertebra detection by z height
upper_nodes= HEALTHYMESH2(z>686); % Upper nodes are the
nodes above 686 height
lower_nodes= HEALTHYMESH2(z<678); % Lower nodes are the
nodes below 678 height

% Vertebra centroids (based on the equation of figure 27)
G1 =
sum(HEALTHYMESH2(upper_nodes,2:4))/length(HEALTHYMESH2(upper
_nodes,2:4));
G2 =
sum(HEALTHYMESH2(lower_nodes,2:4))/length(HEALTHYMESH2(lower
_nodes,2:4));


%% Flexion ROM calculation
% Extracting the nodes displacement
load('flexion_healthy.mat');

% Coordinates of the nodes after the motion
k=1;
for i=1:length(lower_nodes)
    if find(flexion_healthy==lower_nodes(i)) ~=0
```

```
    flexion_nodes(i,:) = HEALTHYMESH2(lower_nodes(i),2:4) +
flexion_healthy(find(flexion_healthy==lower_nodes(i),1),2:4)
; % For the lower nodes, it is added the coordinates of the
displacement of each node
    k=k+1;
    end
end

% Centroids of the nodes after the motion
G11f = G1; % The centroid of the upper vertebra is the same
because is fixed in every direction
G21f = sum(flexion_nodes)/length(flexion_nodes); % Based on
the equation of figure 27

% Flexion angle calculation (based on the equation from
section 2.4.2.1.)
alpha_flexion = acos((dot((G2-G1),(G21f-G11f)))/(norm(G2-
G1)*norm(G21f-G11f)))*180/pi

% Flexion translation calculation
translation_flexion = G21f-G2

%% Extension ROM
% Extracting the nodes displacement
load('extension_healthy.mat');

% Coordinates of the nodes after the motion
k=1;
for i=1:length(lower_nodes)
    if find(extension_healthy==lower_nodes(i)) ~=0
    extension_nodes(i,:) = HEALTHYMESH2(lower_nodes(i),2:4)
+
extension_healthy(find(extension_healthy==lower_nodes(i),1),
2:4); % For the lower nodes, it is added the coordinates of
the displacement of each node
    k=k+1;
    end
end

% Centroids of the nodes after the motion
G11e = G1; % The centroid of the upper vertebra is the same
because is fixed in every direction
G21e = sum(extension_nodes)/length(extension_nodes); % Based
on the equation of figure 27
```

```
% Extension angle calculation (based on the equation from
section 2.4.2.1.)
alpha_extension = acos((dot((G2-G1),(G21e-G11e)))/(norm(G2-
G1)*norm(G21e-G11e)))*180/pi

% Flexion translation calculation
translation_extension = G21e-G2


%% LB ROM
% Extracting the nodes displacement
load('lb_healthy.mat');

% Coordinates of the nodes after the motion
k=1;
for i=1:length(lower_nodes)
    if find(lb_healthy==lower_nodes(i)) ~=0
    LB_nodes(i,:) = HEALTHYMESH2(lower_nodes(i),2:4) +
lb_healthy(find(lb_healthy==lower_nodes(i),1),2:4); % For
the lower nodes, it is added the coordinates of the
displacement of each node
    k=k+1;
    end
end

% Centroids
G11lb = G1; % The centroid of the upper vertebra is the same
because is fixed in every direction
G21lb = sum(LB_nodes)/length(LB_nodes); % Based on the
equation of figure 27

% Lateral bending angle calculation (based on the equation
from section 2.4.2.1.)
alpha_lb = acos((dot((G2-G1),(G21lb-G11lb)))/(norm(G2-
G1)*norm(G21lb-G11lb)))*180/pi

% Lateral bending translation calculation
translation_lb = G21lb-G2
```